

## A Site-Specific ImmunoPET Tracer to Image PD-L1

Haley L. Wissler, Emily B Ehlerding, Zhigang Lyu, Yue Zhao, Si Zhang, Anisa Eshraghi, Zakey Yusuf Buuh, Jeffrey C McGuth, Yifu Guan, Jonathan W Engle, Sarah J Bartlett, Vincent A. Voelz, Weibo Cai, and Rongsheng E. Wang

*Mol. Pharmaceutics*, **Just Accepted Manuscript** • DOI: 10.1021/acs.molpharmaceut.9b00010 • Publication Date (Web): 15 Mar 2019

Downloaded from <http://pubs.acs.org> on March 17, 2019

### Just Accepted

“Just Accepted” manuscripts have been peer-reviewed and accepted for publication. They are posted online prior to technical editing, formatting for publication and author proofing. The American Chemical Society provides “Just Accepted” as a service to the research community to expedite the dissemination of scientific material as soon as possible after acceptance. “Just Accepted” manuscripts appear in full in PDF format accompanied by an HTML abstract. “Just Accepted” manuscripts have been fully peer reviewed, but should not be considered the official version of record. They are citable by the Digital Object Identifier (DOI®). “Just Accepted” is an optional service offered to authors. Therefore, the “Just Accepted” Web site may not include all articles that will be published in the journal. After a manuscript is technically edited and formatted, it will be removed from the “Just Accepted” Web site and published as an ASAP article. Note that technical editing may introduce minor changes to the manuscript text and/or graphics which could affect content, and all legal disclaimers and ethical guidelines that apply to the journal pertain. ACS cannot be held responsible for errors or consequences arising from the use of information contained in these “Just Accepted” manuscripts.



## A Site-Specific ImmunoPET Tracer to Image PD-L1

Haley L. Wissler<sup>1,†</sup>, Emily B. Ehlerding<sup>2,†</sup>, Zhigang Lyu<sup>1</sup>, Yue Zhao<sup>1</sup>, Si Zhang<sup>1</sup>, Anisa Eshraghi<sup>1</sup>, Zakey Yusuf Buuh<sup>1</sup>, Jeffrey C. McGuth<sup>1</sup>, Yifu Guan<sup>1</sup>, Jonathan W. Engle<sup>2</sup>, Sarah J. Bartlett<sup>1</sup>, Vincent A. Voelz<sup>1</sup>, Weibo Cai<sup>2,\*</sup>, Rongsheng E. Wang<sup>1,\*</sup>

1. *Department of Chemistry, Temple University, 1901 N. 13<sup>th</sup> Street, Philadelphia, PA, 19122, USA*

2. *Departments of Radiology and Medical Physics, University of Wisconsin-Madison, WI, 53705, USA*

\* To whom correspondence should be addressed:

Weibo Cai, Phone (608) 262-1749. Email: [wcai@uwhealth.org](mailto:wcai@uwhealth.org)

Rongsheng E. Wang, Phone (215) 204-1855. Email: [rosswang@temple.edu](mailto:rosswang@temple.edu)

† These authors contributed equally.

**ABSTRACT**

The rapid ascension of immune checkpoint blockade treatments has placed an emphasis on the need for viable, robust, and noninvasive imaging methods for immune checkpoint proteins, which could be of diagnostic value. Immunoconjugate-based positron emission tomography (immuno-PET) allows for sensitive and quantitative imaging of target levels and has promising potential for the noninvasive evaluation of immune checkpoint proteins. However, the advancement of immuno-PET is currently limited by available imaging tools, which heavily rely on full-length IgGs with Fc-mediated effects and are heterogeneous mixtures upon random conjugation with chelators for imaging. Herein, we have developed a site-specific  $\alpha$ PD-L1 Fab conjugate with the chelator NOTA, enabling radiolabeling for PET imaging, using the amber suppression-mediated genetic incorporation of unnatural amino acid (UAA), p-azidophenylalanine. This Fab conjugate is homogeneous and demonstrated tight binding towards the PD-L1 antigen *in vitro*. The radiolabeled version,  $^{64}\text{Cu}$ -NOTA- $\alpha$ PD-L1, has been employed in PET imaging to allow for effective visualization and mapping of the biodistribution of PD-L1 in two normal mouse models, including the capturing of different PD-L1 expression levels in the spleens of the different mouse types. Follow-up *in vivo* blocking studies and *ex vivo* fluorescent staining further validated specific tissue uptakes of the imaging agent. This approach illustrates the utility of UAA-based site-specific Fab conjugation as a general strategy for making sensitive PET imaging probes, which could facilitate the elucidation of the roles of a wide variety of immune checkpoint proteins in immunotherapy.

**KEYWORDS**

Antibody, Immune checkpoint, Immunotherapy, PD-L1, Site-specific, Positron Emission Tomography, Unnatural amino acid.

## INTRODUCTION

Checkpoint inhibitor-based cancer immunotherapy has recently emerged as a pillar of effective treatment to control tumor growth and dissemination.<sup>1, 2</sup> The discovery of multiple immune checkpoint mechanisms such as program death-ligand 1 (PD-L1), programmed cell death protein 1 (PD-1), and cytotoxic T-lymphocyte-associated protein 4 (CTLA-4) has facilitated the understanding of how tumor cells bypass the attack of immune systems.<sup>3</sup> Therapeutic treatments utilizing immune checkpoint inhibitors would ‘wake up’ the previously suppressed immune cells and activate them to attack tumor cells.<sup>3</sup> Thus, these inhibitors such as antibodies, have become first-line therapies for different tumor types.<sup>1, 3</sup> Yet, heterogeneous outcomes in clinical responses, frequent toxicity, and adverse effects necessitate the development of new methods for the prognosis and monitoring of patient responses.<sup>1, 2, 4-8</sup> A non-invasive strategy to comprehensively monitor the expression of immune checkpoint proteins may help elucidate their roles in immunotherapeutic responses, and potentially be useful in patient selection and treatment monitoring.<sup>4, 9-13</sup> Molecular imaging, especially positron emission tomography using antibodies conjugated with radionuclides (Immuno-PET), allows for accurate and non-invasive evaluation of target levels.<sup>14-16</sup> Due to high sensitivity and resolution, immuno-PET has been successfully applied to interrogate the relation between tissue uptake and clinical responses towards antibody treatment.<sup>17-19</sup> Thus, immuno-PET could be a crucial tool to test the biomarker hypothesis of immune checkpoint proteins for immunotherapy.<sup>15, 16, 20</sup>

Despite previous PET imaging efforts for immune checkpoint proteins,<sup>9-11, 20-26</sup> most immune-checkpoint-based PET probes rely on full-length IgG antibodies,<sup>10, 21, 23, 24</sup> which have limited tissue/tumor penetrance. Fab fragments on the other hand, retain the binding of the antibody but

1  
2  
3 are devoid of the Fc effector domain. The resulting shorter circulation half-lives and less off-  
4 target-related background signals make them ideal probe candidates.<sup>27, 28</sup> Yet, few Fab-based PET  
5 probes have been developed so far.<sup>27, 28</sup> More importantly, common antibody probes have been  
6 synthesized via random coupling of natural amino acids with chelators, resulting in heterogeneous  
7 constructs with suboptimal stabilities, efficacies, and pharmacological properties.<sup>29, 30</sup> Early  
8 studies with cysteine-based site-specific immunoconjugates revealed higher target-to-background  
9 imaging intensity ratios than random conjugates,<sup>30</sup> demonstrating the positive effects on *in vivo*  
10 performance of precise control of conjugation sites and stoichiometry. Yet, the suboptimal  
11 biological stability of the resulting maleimide thioether bonds largely limited its broad  
12 applications.<sup>30</sup> Another cysteine-based approach, expressed protein ligation (EPL), could result in  
13 relatively stable coupling, but the feasible site is mainly limited to C-terminals which may not  
14 render the most stable conjugates.<sup>31</sup> On the other hand, application of EPL to multiple  
15 modifications within the protein sequence would be technically demanding.<sup>32, 33</sup> Recently, another  
16 site-specific conjugation strategy emerged, with the amber suppression-mediated genetic  
17 incorporation of unnatural amino acids (UAA) during the translation of recombinant proteins.<sup>33, 34</sup>  
18 In this approach, the amber stop codon employs paired orthogonal amino-acyl transferase and iso-  
19 tRNA to incorporate the desired UAA site specifically into proteins including the recombinant  
20 antibody.<sup>33, 34</sup> Antibodies incorporating UAAs such as p-acetylphenylalanine (pAcF) can be  
21 coupled to small molecules of interest via a stable linkage,<sup>29, 35, 36</sup> generating site-specific  
22 therapeutics in high yields. The UAA conjugates as therapeutic candidates have demonstrated  
23 superior *in vivo* efficacy, stability, and toxicology profiles to the cysteine conjugates.<sup>34, 37, 38</sup>  
24 Nevertheless, UAA-incorporated immunoconjugates have rarely been applied to PET imaging.<sup>29,</sup>

25  
26  
27  
28  
29  
30  
31  
32  
33  
34  
35  
36  
37  
38  
39  
40  
41  
42  
43  
44  
45  
46  
47  
48  
49  
50  
51  
52  
53  
54  
55  
56  
57  
58  
59  
60

To this end, we have developed a site-specific immuno-PET probe by incorporating one UAA, p-azidophenylalanine (pAzF), into antibody Fab fragments. Using the antibody against the popularly studied immune checkpoint protein PD-L1 as an example, we demonstrated for the first time the generation, optimization, and *in vivo* PET imaging of a UAA-based site-specific Fab conjugate with 1,4,7-triazacyclononane-N, N',N''-triacetic acid (NOTA).

## EXPERIMENTAL SECTION

**Materials.** Reagents and solvents were obtained directly from commercial resources such as Thermo Fisher, VWR, and Sigma Aldrich, and were used without further purification. Analytical thin-layer chromatography was performed with EMD Chemicals Silica gel 60 F<sub>254</sub> plates, the chemicals on which were visualized by UV lamp (Chemglass Life Sciences) at 254/365 nm, KMnO<sub>4</sub> staining, or PMA staining. For purification, flash column chromatography was performed with silica gel grade 60 (230-400 mesh, Fisher Scientific). Preparative HPLC was carried out on Waters 1525 series equipped with a 2489 UV/vis detector, 1525 binary pump, and a XBridge Prep C18 column (5 μm, 19×250 mm). Solvent A was water/0.5% trifluoroacetic acid (TFA), and solvent B was acetonitrile. For mass spectrometry analysis, regular liquid chromatography-mass spectrometry (LC-MS) was performed on Agilent 1100 series. High resolution LC-MS analysis was done on an Agilent 6520 Accurate-Mass Quadrupole-Time-of-Flight (Q-TOF) coupled with an electrospray ionization (ESI) source. A zorbax 300SB-C8 column (5μm, 4.6×50 mm) was used. For acquisition of NMR spectroscopy, <sup>1</sup>HNMR and <sup>13</sup>CNMR were recorded on 400 MHz or 500 MHz Bruker Advance. The data were processed with the MestReNova Software, measuring signal shifts in parts per million (ppm) downfield from the internal standard tetramethyl silane (TMS).

**Methods.** Please see the Supporting Information for experimental details.

## RESULTS AND DISCUSSION

**Synthesis of the NOTA-BCN Linker.** We began by designing and synthesizing the PET chelator. Copper-64 as a metallic radionuclide garners interest due to its favorable physical properties, appropriate half-life and ease of production.<sup>40-43</sup> Among the available macrocyclic chelates, the NOTA series have been reported to possess superior chelation ability.<sup>40</sup> Notably, the hexadentate NOTA derivative with 1-branched substitution (3p-C-NOTA) had higher radiolabeling efficiency and stability than the other NOTA derivatives,<sup>40</sup> but has yet to be utilized for immuno-PET.<sup>44-46</sup> Thus, we set out to synthesize a similar NOTA derivative with the termini modified with bicyclo[6.1.0]non-4-yne (BCN) for strain-promoted azide-alkyne cycloaddition (SPAAC) conjugation.<sup>47</sup> 6-benzamidohexanoic acid was first reacted with benzoyl chloride to afford protected linker compound **1** (Scheme 1).<sup>48</sup> Bromination followed by methylation resulted in methyl 6-benzamido-2-bromohexanoate (compound **2**). The 1,4,7-triazacyclononane (TACN) moiety was introduced by reacting the linker compound **2** with TACN-1,7-bis(t-butyl acetate) in the presence of potassium carbonate.<sup>45, 48</sup> The resulting intermediate was hydrolyzed under strong acid conditions to generate the amine derivatized NOTA compound **3**. A final coupling of **3** with the BCN-succinimidyl ester, followed by HPLC purification, afforded the NOTA-BCN linker (compound **4**) with > 95% purity, as shown by LC-MS analysis (Supplementary Information Figure S1).

**Design and Synthesis of Anti-PD-L1 Fab Mutant.** Compared to IgGs, antibody Fab fragments possess a small protein size thereby improving tissue penetrance, and the removal of the Fc portion avoids unwanted effector effects.<sup>27, 28</sup> Its shorter biological half-life enables labeling with shorter-lived radionuclides such as copper-64, which taken together should lead to improved signal-to-

1  
2  
3 background ratios at earlier time points.<sup>27</sup> These unique characteristics make them not only  
4  
5 suitable for therapeutic development,<sup>49, 50</sup> but also as ideal imaging agents,<sup>27</sup> warranting a detailed  
6  
7 test of the site-specific incorporation of UAA. Among all the available immune checkpoint  
8  
9 proteins, PD-L1 appears to be the most studied due to its broad and dynamic expression profile  
10  
11 and its potential correlation with prognosis and therapy responsiveness.<sup>10, 20, 21, 23, 24, 26</sup> Hence, we  
12  
13 picked the sequences coding for the variable regions of the  $\alpha$ PD-L1 antibody avelumab, which has  
14  
15 been clinically approved for treating gastric cancer and Merkel-cell carcinoma, and is also human-  
16  
17 mouse cross-reactive.<sup>51</sup> The plasmid (pBAD\_ $\alpha$ PD-L1) was constructed to harbor the heavy- and  
18  
19 lambda light-chain genes of the Fab fragment following a still signal peptide.<sup>36, 52</sup> The wild type  
20  
21  $\alpha$ PD-L1 Fab was expressed in *E. coli*, with a yield of 4.2 mg/L in shake flask cultures. SDS/PAGE  
22  
23 analysis showed that the Fab fragment migrated as a single band, with > 95% purity and a  
24  
25 molecular mass of ~ 45 kDa (Figure S2).  
26  
27  
28  
29  
30  
31  
32

33 The site-specific labeling strategy based on the genetic incorporation of UAA allows one to  
34  
35 explore various conjugates with different geometries and stabilities.<sup>36, 52</sup> Previous studies on a  
36  
37 couple of mutation sites have resulted in Fab fragments of significantly different yields.<sup>36</sup>  
38  
39 Nevertheless, there has been no systematic study done to determine the optimal conjugation site.  
40  
41 To this end, we selected 23 possible sites on  $\alpha$ PD-L1 Fab, which are surface-exposed, distal to  
42  
43 binding sites, and are in flexible loops (Figure 1A). In silico screening was performed using the  
44  
45 RosettaBackrub algorithm to predict the viability of single point mutations at the selected sites  
46  
47 (Figure 2). The results suggested that mutations at HC-K129 would be most favorably tolerated  
48  
49 (Figure 2). Notably, the site HC-K129 has been experimentally explored before to be an ideal  
50  
51 conjugation site for pAcF with high expression yield, and little interference with antigen binding.<sup>36</sup>  
52  
53  
54  
55  
56  
57  
58  
59  
60

1  
2  
3 <sup>52, 53</sup> As a negative control in our experimental validation of the screening results, LC-V202 was  
4  
5  
6 picked for amber suppression as well. Despite the previous site-specific incorporation of pAcF  
7  
8 for oxime coupling,<sup>36</sup> we decided to employ the incorporation of pAzF for strain-promoted  
9  
10 SPAAC in this study. Compared to oxime coupling, the strain-promoted SPAAC conjugation is  
11  
12 more bioorthogonal, and can proceed efficiently at neutral pH.<sup>39, 54, 55</sup> Although there are few  
13  
14 reports in regards to its incorporation onto antibodies,<sup>54</sup> electron-deficient aryl azides such as pAzF  
15  
16 have been shown to greatly accelerate the SPAAC reaction.<sup>47</sup>  
17  
18  
19  
20

21  
22 Therefore, we performed site-directed mutation of HC-K129 or LC-V202 to the TAG codon,  
23  
24 and cotransformed each pBAD plasmid into the DH10B strain along with a plasmid  
25  
26 (pULTRA\_pCNF)<sup>56</sup> that encodes the polyspecific Mj-tRNA/tyrosyl-tRNA synthetase pair evolved  
27  
28 to incorporate the pAzF UAA. The expression yield for  $\alpha$ PD-L1 Fab mutant (HC K129X, X =  
29  
30 pAzF) was 2.5 mg/L, while the yield for  $\alpha$ PD-L1 Fab (LC V202X, X = pAzF) was only 0.04 mg/L.  
31  
32 This significant difference is consistent with the in-silico screening results, and emphasizes the  
33  
34 importance of optimizing the labeling site. In parallel, we also cloned and expressed  $\alpha$ HER2 Fab  
35  
36 mutant (HC K129X, X = pAzF), which could serve as a non-relevant antibody control for follow-  
37  
38 up imaging experiments. Both Fab antibodies migrated as a single band on SDS/PAGE analysis,  
39  
40 indicating a > 95% purity, and a molecular weight of ~ 45 kDa (Figure S2). Their identities were  
41  
42 further confirmed by ESI-MS analysis (Figure S3).  
43  
44  
45  
46  
47  
48

49 **Synthesis and Characterization of Site-Specific NOTA-Anti-PD-L1 Fab Conjugate.** Next,  
50  
51 we conjugated the purified Fab mutants ( $\alpha$ PD-L1 Fab and  $\alpha$ HER2 Fab, HC K129X, X = pAzF)  
52  
53 with linker compound **4** (Figure 1A). Each pAzF-containing Fab was reacted with a 10-fold  
54  
55  
56  
57  
58  
59  
60

1  
2  
3 excess of NOTA-BCN linker at 37 °C for 12 h to ensure the complete conjugation. The Fab  
4 conjugates were purified following the reported procedures,<sup>36, 57</sup> and analyzed by SDS/PAGE  
5 (Figure S2) and ESI-MS (Figure S3), which demonstrated that the final conjugates were > 95%  
6 pure, and had the desired molecular mass with a NOTA-to-antibody ratio of 1 (Figure S3). The  
7 binding affinity of  $\alpha$ PD-L1 Fab fragments to PD-L1 was evaluated by ELISA (Figure 1B). The  
8 conjugate and the HC K129 mutant both have a similar affinity ( $EC_{50}$ 's  $\sim$  0.7 nM) to the wild type,  
9 suggesting that neither the site-directed mutation nor payload conjugation at the selected site  
10 compromises the antibody's binding.  
11  
12  
13  
14  
15  
16  
17  
18  
19  
20  
21  
22  
23

24 ***In vivo* PET Imaging of PD-L1 Expression.** To utilize this class of site-specific Fab conjugates  
25 as imaging probes, we evaluated their *in vivo* PET imaging capability using nude mice that are  
26 immuno-deficient and can potentially carry various tumor types for future studies.<sup>58-60</sup> After  
27 radiolabeling with  $^{64}\text{Cu}$ , 50 – 70  $\mu\text{Ci}$  of either  $^{64}\text{Cu}$ -NOTA- $\alpha$ PD-L1 or  $^{64}\text{Cu}$ -NOTA- $\alpha$ HER2 were  
28 intravenously administered to nude mice. PET scans were performed at 5, 15, and 45 min  
29 postinjection (p.i.). As demonstrated by Figure 3A, PET signal vs. noise became stable at 45 min  
30 p.i., with background signals almost cleared. Compared to the intact full length antibody  
31 counterparts,<sup>10, 23</sup> Fab fragment-based PET agents provided higher contrast imaging due to the low  
32 level of nonspecific accumulation and faster clearance mechanisms,<sup>61</sup> potentially ideal for imaging  
33 highly abundant surface markers. Fab conjugates were mostly cleared through the renal pathway  
34 and excreted via the urinary bladder, as evidenced by the extremely high kidney and bladder  
35 uptakes. Both images (Figure 3A) and region-of-interest (ROI) analysis (Figure 3B, 3C) revealed  
36 specific uptake of  $^{64}\text{Cu}$ -NOTA- $\alpha$ PD-L1 in brown adipose tissue (BAT) and spleen. For BAT, the  
37 accumulation of  $^{64}\text{Cu}$ -NOTA- $\alpha$ PD-L1 was highest immediately after injection ( $6.2 \pm 2.4$  %ID/g,  
38  
39  
40  
41  
42  
43  
44  
45  
46  
47  
48  
49  
50  
51  
52  
53  
54  
55  
56  
57  
58  
59  
60

1  
2  
3 n = 3) and remained high throughout the study ( $6.1 \pm 2.1$  %ID/g at 45 min). The control  $^{64}\text{Cu}$ -  
4  
5  
6  
7  
8  
9  
10  
11  
12  
13  
14  
15  
16  
17  
18  
19  
20  
21  
22  
23  
24  
25  
26  
27  
28  
29  
30  
31  
32  
33  
34  
35  
36  
37  
38  
39  
40  
41  
42  
43  
44  
45  
46  
47  
48  
49  
50  
51  
52  
53  
54  
55  
56  
57  
58  
59  
60  
NOTA- $\alpha\text{HER2}$ , on the contrary, displayed minimal enrichment in BAT, from  $1.7 \pm 0.2$  %ID/g at  
15 min to  $1.6 \pm 0.1$  %ID/g at 45 min ( $n = 3$ ). For the spleen, there was a similar trend for  $^{64}\text{Cu}$ -  
NOTA- $\alpha\text{PD-L1}$  ( $11.8 \pm 3.0$  %ID/g at 15 min to  $12.0 \pm 1.9$  %ID/g at 45 min,  $n = 3$ ), while the  
uptake of the control  $^{64}\text{Cu}$ -NOTA- $\alpha\text{HER2}$  ( $2.5 \pm 0.1$  %ID/g at 15 min to  $2.1 \pm 0.3$  %ID/g at 45  
min,  $n = 3$ ) remained low. These resulted in statistically significant differences ( $p < 0.05$ ) in both  
BAT and spleen uptake for the two imaging tracers at the time point of 45 min p.i. (Figure 3B,  
3C), while there was no notable difference in other analyzed organs.

To further confirm that the observed enrichment of  $^{64}\text{Cu}$ -NOTA- $\alpha\text{PD-L1}$  is antigen-specific, we  
performed blocking studies in nude mice by injecting wild type  $\alpha\text{PD-L1}$  Fab at a dose of  $\sim 200$   
 $\mu\text{g}/\text{mouse}$  prior to the administration of the corresponding NOTA conjugate. As shown in Figures  
3B and 3C, the uptake of the NOTA conjugate was drastically decreased in both BAT ( $1.9 \pm$   
 $0.3$  %ID/g at 15 min and  $1.4 \pm 0.3$  %ID/g at 45 min,  $n = 3$ ) and spleen ( $3.8 \pm 0.3$  %ID/g at 15 min  
and  $1.7 \pm 1.2$  %ID/g at 45 min,  $n = 3$ ), similar to the levels of the control  $\alpha\text{HER2}$  conjugate. Taken  
together, this set of results indicate that the uptake of PET tracer in BAT and spleen of nude mice  
was PD-L1 specific. This finding suggests that the  $^{64}\text{Cu}$ -NOTA- $\alpha\text{PD-L1}$  probe is a reliable, non-  
metabolic tracer for *in vivo* PD-L1 expression. PD-L1 checkpoint was initially regarded to be  
primarily expressed in the extralymphatic organs.<sup>3, 10</sup> The existence of PD-L1 in the spleen is  
consistent with recent findings that PD-L1 is additionally expressed in secondary lymphatic  
organs.<sup>10</sup> The presence of PD-L1 in BAT further confirms that adipose tissue is influenced by  
arms of the immune system.<sup>10, 21, 62</sup> These organs' expression of PD-L1 may suggest their  
utilization of PD-1/PD-L1 interactions to locally suppress unwanted T-cell responses.<sup>10</sup>

1  
2  
3  
4  
5  
6 Next, we set out to gauge the general applicability of our imaging probe in another mouse model,  
7  
8 C57BL/6 mice that are immunocompetent. Similarly, the BAT and spleen were found to have  
9  
10 much higher accumulation of  $^{64}\text{Cu}$ -NOTA- $\alpha$ PD-L1 than that of the control  $^{64}\text{Cu}$ -NOTA- $\alpha$ HER2  
11  
12 throughout the study (Figure S4). The uptake of  $^{64}\text{Cu}$ -NOTA- $\alpha$ PD-L1 in the spleen was less  
13  
14 significant (Figures S4A, S4C), presumably due to the more varied expression levels of PD-L1 in  
15  
16 the spleens among individual C57BL/6 mice (Figure S4A, S4C).<sup>10, 63, 64</sup> This observation may  
17  
18 accurately reflect the real situation, which in translation to the clinical situation, may partially  
19  
20 account for heterogeneous immunotherapeutic responses.  
21  
22

23  
24  
25  
26 ***Ex vivo* Biodistribution Studies and Immunofluorescence Staining.** Following the last PET  
27  
28 scan at 90 min p.i., C57BL/6 mice were sacrificed, with major organs resected for *ex vivo* gamma  
29  
30 counting to corroborate the quantification of PET images (Figure S5). The kidneys from both  
31  
32 groups had extremely high accumulation of the tracers, at  $157 \pm 27$  %ID/g for  $^{64}\text{Cu}$ -NOTA- $\alpha$ PD-  
33  
34 L1 and  $219 \pm 28$  %ID/g for  $^{64}\text{Cu}$ -NOTA- $\alpha$ Her2. Low but specific tracer uptake in the lung and  
35  
36 intestines were also revealed, consistent with the reported PD-L1 expression in minor cell  
37  
38 populations.<sup>10</sup> Notably, the biodistribution data corroborated the findings from *in vivo* PET ROI  
39  
40 analysis. The BAT uptakes with the two imaging agents were significantly different from one  
41  
42 another in this analysis as well ( $4.5 \pm 1.5$  %ID/g for  $^{64}\text{Cu}$ -NOTA- $\alpha$ PD-L1 and  $0.9 \pm 0.2$  %ID/g for  
43  
44  $^{64}\text{Cu}$ -NOTA- $\alpha$ HER2,  $p < 0.05$ ). The enrichment of  $^{64}\text{Cu}$ -NOTA- $\alpha$ PD-L1 was still higher than the  
45  
46 control in spleen ( $9.4 \pm 3.9$  %ID/g vs.  $2.3 \pm 0.8$  %ID/g), but with large variations. Follow-up  
47  
48 immunofluorescent staining of these organs further confirmed that both BAT and spleen are PD-  
49  
50 L1 positive (Figure 4). These results are consistent with recent literature reports,<sup>9, 10, 21, 24, 26</sup> which  
51  
52  
53  
54  
55  
56  
57  
58  
59  
60

1  
2  
3 suggests the tissue-specific (BAT, spleen) uptake of antibodies against PD-L1, and indicates that  
4  
5 our  $^{64}\text{Cu}$ -NOTA- $\alpha$ PD-L1 probe is highly specific towards PD-L1.  
6  
7  
8  
9

10 **In Conclusion:** We have developed and studied a  $^{64}\text{Cu}$ -labeled, UAA-based, site-specific Fab  
11 conjugate as an imaging probe to measure PD-L1 expression levels *in vivo* with immunoPET. This  
12 antibody conjugate was optimized at a fixed site and stoichiometry, and bears an indistinguishable  
13 binding affinity from the unconjugated wild type towards the cognate antigen. When applied to  
14 noninvasive *in vivo* imaging, the probe can sensitively detect the expression levels of the targeted  
15 antigen, in different mouse models. The particular PD-L1 expression on non-tumor organs, such  
16 as BAT, lung, and intestines, as revealed by this probe, may indicate that targeted T cell responses  
17 in these organs are strongly suppressed by the PD1/PD-L1 immune checkpoint.<sup>10</sup> Further, these  
18 findings may explain the frequent association of immune checkpoint blockade with immune-  
19 related adverse effects on these organs,<sup>10</sup> underlying the importance of image-guided prognosis  
20 and treatment monitoring in immunotherapy. These data generally support the hypothesis that  
21 imaging PD-L1 expression with UAA-based site-specific Fab conjugates may be feasible in future  
22 clinical settings. Further evaluation of the conjugate in disease-related models (xenograft and  
23 syngeneic tumor models) will be required to determine its clinical potential. In addition, we are  
24 comparing the properties and activity of this conjugate with random conjugates and cysteine-based  
25 site-specific conjugates. Finally, this work suggests that the amber-suppression mediated genetic  
26 incorporation strategy has applicability as a route to a class of site-specific immuno-PET probes  
27 that can potentially guide immune checkpoint-targeted immunotherapy.  
28  
29  
30  
31  
32  
33  
34  
35  
36  
37  
38  
39  
40  
41  
42  
43  
44  
45  
46  
47  
48  
49  
50  
51  
52  
53

## 54 ASSOCIATED CONTENT

55  
56  
57  
58  
59  
60

1  
2  
3 The Supporting Information is available free of charge on the ACS Publications website at DOI:  
4  
5 Supporting Figures (S1 – S5) and detailed descriptions of the experimental methods applied in this  
6  
7 study (PDF).  
8  
9  
10  
11

## 12 **AUTHOR INFORMATION**

### 14 **Corresponding Authors**

15 \*Phone: 608-262-1749, E-mail: wcai@uwhealth.org

16 \*Phone: 215-204-1855, E-mail: rosswang@temple.edu

### 18 **Notes**

19 The authors declare no competing financial interest.  
20  
21  
22  
23  
24  
25  
26  
27  
28

## 29 **ACKNOWLEDGMENTS**

30  
31  
32 This work was supported by grant #15-175-22 from the American Cancer Society, Temple  
33  
34 University Startup Fund, and was also supported, in part, by the University of Wisconsin-Madison  
35  
36 and the National Institutes of Health (P30CA014520, T32GM008505, T32CA009206). V.V. and  
37  
38 S.Z. were supported by National Institutes of Health (NIH) grant 1R01GM123296.  
39  
40  
41  
42  
43  
44  
45  
46  
47  
48  
49  
50  
51  
52  
53  
54  
55  
56  
57  
58  
59  
60

**REFERENCES**

- 1  
2  
3  
4  
5  
6  
7  
8  
9  
10  
11  
12  
13  
14  
15  
16  
17  
18  
19  
20  
21  
22  
23  
24  
25  
26  
27  
28  
29  
30  
31  
32  
33  
34  
35  
36  
37  
38  
39  
40  
41  
42  
43  
44  
45  
46  
47  
48  
49  
50  
51  
52  
53  
54  
55  
56  
57  
58  
59  
60
- (1) Burugu, S., Dancsok, A. R., and Nielsen, T. O. (2018) Emerging targets in cancer immunotherapy, *Semin. Cancer Biol.* 52(Pt 2): 39-52.
- (2) Davies, M., and Duffield, E. A. (2017) Safety of checkpoint inhibitors for cancer treatment: strategies for patient monitoring and management of immune-mediated adverse events, *Immunotargets Ther.* 6, 51-71.
- (3) Pardoll, D. M. (2012) The blockade of immune checkpoints in cancer immunotherapy, *Nat Rev Cancer* 12, 252-264.
- (4) Aris, M., Mordoh, J., and Barrio, M. M. (2017) Immunomodulatory Monoclonal Antibodies in Combined Immunotherapy Trials for Cutaneous Melanoma, *Front. Immunol.* 8, 1024.
- (5) Voutsadakis, I. A. (2016) Immune Blockade Inhibition in Breast Cancer, *Anticancer Res.* 36, 5607-5622.
- (6) Moslehi, J. J., Salem, J. E., Sosman, J. A., Lebrun-Vignes, B., and Johnson, D. B. (2018) Increased reporting of fatal immune checkpoint inhibitor-associated myocarditis, *Lancet.* 391, 933.
- (7) Johnson, D. B., Balko, J. M., Compton, M. L., Chalkias, S., Gorham, J., Xu, Y., Hicks, M., Puzanov, I., Alexander, M. R., Bloomer, T. L., Becker, J. R., Slosky, D. A., Phillips, E. J., Pilkinton, M. A., Craig-Owens, L., Kola, N., Plautz, G., Reshef, D. S., Deutsch, J. S., Deering, R. P., Olenchock, B. A., Lichtman, A. H., Roden, D. M., Seidman, C. E., Koralnik, I. J., Seidman, J. G., Hoffman, R. D., Taube, J. M., Diaz, L. A., Jr., Anders, R. A., Sosman, J. A., and Moslehi, J. J. (2016) Fulminant Myocarditis with Combination Immune Checkpoint Blockade, *N. Engl. J. Med.* 375, 1749-1755.
- (8) Leem, G., and Song, S. Y. (2016) Immunotherapy in Pancreatic Cancer; the Road Less Traveled, *Immunol. Disord. Immunother.* 1, 1000106.
- (9) Ingram, J. R., Dougan, M., Rashidian, M., Knoll, M., Keliher, E. J., Garrett, S., Garforth, S., Blomberg, O. S., Espinosa, C., Bhan, A., Almo, S. C., Weissleder, R., Lodish, H., Dougan, S. K., and Ploegh, H. L. (2017) PD-L1 is an activation-independent marker of brown adipocytes, *Nat. Commun.* 8, 647.
- (10) Hettich, M., Braun, F., Bartholoma, M. D., Schirmbeck, R., and Niedermann, G. (2016) High-Resolution PET Imaging with Therapeutic Antibody-based PD-1/PD-L1 Checkpoint Tracers, *Theranostics* 6, 1629-1640.
- (11) Natarajan, A., Mayer, A. T., Xu, L., Reeves, R. E., Gano, J., and Gambhir, S. S. (2015) Novel Radiotracer for ImmunoPET Imaging of PD-1 Checkpoint Expression on Tumor Infiltrating Lymphocytes, *Bioconjug. Chem.* 26, 2062-2069.

- 1  
2  
3 (12) Rom-Jurek, E. M., Kirchhammer, N., Ugocsai, P., Ortmann, O., Wege, A. K., and Brockhoff,  
4 G. (2018) Regulation of Programmed Death Ligand 1 (PD-L1) Expression in Breast Cancer Cell  
5 Lines In Vitro and in Immunodeficient and Humanized Tumor Mice, *Int. J. Mol. Sci.* 19, pii:E563.  
6  
7  
8 (13) Sabatier, R., Finetti, P., Mamessier, E., Adelaide, J., Chaffanet, M., Ali, H. R., Viens, P.,  
9 Caldas, C., Birnbaum, D., and Bertucci, F. (2015) Prognostic and predictive value of PDL1  
10 expression in breast cancer, *Oncotarget* 6, 5449-5464.  
11  
12 (14) Ehlerding, E. B., England, C. G., McNeel, D. G., and Cai, W. (2016) Molecular Imaging of  
13 Immunotherapy Targets in Cancer, *J. Nucl. Med.* 57, 1487-1492.  
14  
15  
16 (15) Bauckneht, M., Piva, R., Sambuceti, G., Grossi, F., and Morbelli, S. (2017) Evaluation of  
17 response to immune checkpoint inhibitors: Is there a role for positron emission tomography?,  
18 *World J. Radiol.* 9, 27-33.  
19  
20 (16) Widmann, G., Nguyen, V. A., Plaickner, J., and Jaschke, W. (2016) Imaging Features of  
21 Toxicities by Immune Checkpoint Inhibitors in Cancer Therapy, *Curr. Radiol. Rep.* 5, 59.  
22  
23  
24 (17) Huisman, M., Menke, C., Gootjes, E., Vugts, D., Greuter, H., Boellaard, R., Verheul, H., and  
25 Van Dongen, G. (2014) 89Zr labeled cetuximab imaging in colorectal cancer patients aimed at  
26 image-guided patient selection for anti-EGFR treatment, *J. Nucl. Med.* 55, 225.  
27  
28  
29 (18) Menke-van der Houven van Oordt, C. W., Gootjes, E. C., Huisman, M. C., Vugts, D. J., Roth,  
30 C., Luik, A. M., Mulder, E. R., Schuit, R. C., Boellaard, R., Hoekstra, O. S., van Dongen, G. A.,  
31 and Verheul, H. M. (2015) 89Zr-cetuximab PET imaging in patients with advanced colorectal  
32 cancer, *Oncotarget* 6, 30384-30393.  
33  
34 (19) van Dijk, L. K., Boerman, O. C., Kaanders, J. H., and Bussink, J. (2015) PET Imaging in  
35 Head and Neck Cancer Patients to Monitor Treatment Response: A Future Role for EGFR-  
36 Targeted Imaging, *Clin. Cancer Res.* 21, 3602-3609.  
37  
38  
39 (20) Chatterjee, S., Lesniak, W. G., and Nimmagadda, S. (2017) Noninvasive Imaging of Immune  
40 Checkpoint Ligand PD-L1 in Tumors and Metastases for Guiding Immunotherapy, *Mol. Imaging*  
41 *16*, 1536012117718459.  
42  
43 (21) Chatterjee, S., Lesniak, W. G., Gabrielson, M., Lisok, A., Wharram, B., Sysa-Shah, P., Azad,  
44 B. B., Pomper, M. G., and Nimmagadda, S. (2016) A humanized antibody for imaging immune  
45 checkpoint ligand PD-L1 expression in tumors, *Oncotarget* 7, 10215-10227.  
46  
47  
48 (22) England, C. G., Jiang, D., Ehlerding, E. B., Rekoske, B. T., Ellison, P. A., Hernandez, R.,  
49 Barnhart, T. E., McNeel, D. G., Huang, P., and Cai, W. (2018) (89)Zr-labeled nivolumab for  
50 imaging of T-cell infiltration in a humanized murine model of lung cancer, *Eur. J. Nucl. Med. Mol.*  
51 *Imaging* 45, 110-120.  
52  
53  
54  
55  
56  
57  
58  
59  
60

1  
2  
3 (23) Heskamp, S., Hobo, W., Molkenboer-Kuenen, J. D., Olive, D., Oyen, W. J., Dolstra, H., and  
4 Boerman, O. C. (2015) Noninvasive Imaging of Tumor PD-L1 Expression Using Radiolabeled  
5 Anti-PD-L1 Antibodies, *Cancer Res.* 75, 2928-2936.  
6

7  
8 (24) Josefsson, A., Nedrow, J. R., Park, S., Banerjee, S. R., Rittenbach, A., Jammes, F., Tsui, B.,  
9 and Sgouros, G. (2016) Imaging, Biodistribution, and Dosimetry of Radionuclide-Labeled PD-L1  
10 Antibody in an Immunocompetent Mouse Model of Breast Cancer, *Cancer Res.* 76, 472-479.  
11

12 (25) Natarajan, A., Mayer, A. T., Reeves, R. E., Nagamine, C. M., and Gambhir, S. S. (2017)  
13 Development of Novel ImmunoPET Tracers to Image Human PD-1 Checkpoint Expression on  
14 Tumor-Infiltrating Lymphocytes in a Humanized Mouse Model, *Mol. Imaging Biol.* 19, 903-914.  
15

16  
17 (26) Truillet, C., Oh, H. L. J., Yeo, S. P., Lee, C. Y., Huynh, L. T., Wei, J., Parker, M. F. L.,  
18 Blakely, C., Sevillano, N., Wang, Y. H., Shen, Y. S., Olivas, V., Jami, K. M., Moroz, A., Jego, B.,  
19 Jaumain, E., Fong, L., Craik, C. S., Chang, A. J., Bivona, T. G., Wang, C. I., and Evans, M. J.  
20 (2018) Imaging PD-L1 Expression with ImmunoPET, *Bioconjug. Chem.* 29, 96-103.  
21

22  
23 (27) Ilovich, O., Natarajan, A., Hori, S., Sathirachinda, A., Kimura, R., Srinivasan, A., Gebauer,  
24 M., Kruij, J., Focken, I., Lange, C., Carrez, C., Sassoon, I., Blanc, V., Sarkar, S. K., and Gambhir,  
25 S. S. (2015) Development and Validation of an Immuno-PET Tracer as a Companion Diagnostic  
26 Agent for Antibody-Drug Conjugate Therapy to Target the CA6 Epitope, *Radiology* 276, 191-198.  
27

28  
29 (28) Maute, R. L., Gordon, S. R., Mayer, A. T., McCracken, M. N., Natarajan, A., Ring, N. G.,  
30 Kimura, R., Tsai, J. M., Manglik, A., Kruse, A. C., Gambhir, S. S., Weissman, I. L., and Ring, A.  
31 M. (2015) Engineering high-affinity PD-1 variants for optimized immunotherapy and immuno-  
32 PET imaging, *Proc. Natl. Acad. Sci. U S A* 112, E6506-6514.  
33

34 (29) Adumeau, P., Sharma, S. K., Brent, C., and Zeglis, B. M. (2016) Site-Specifically Labeled  
35 Immunoconjugates for Molecular Imaging--Part 2: Peptide Tags and Unnatural Amino Acids, *Mol.*  
36 *Imaging Biol.* 18, 153-165.  
37

38  
39 (30) Adumeau, P., Sharma, S. K., Brent, C., and Zeglis, B. M. (2016) Site-Specifically Labeled  
40 Immunoconjugates for Molecular Imaging--Part 1: Cysteine Residues and Glycans, *Mol. Imaging*  
41 *Biol.* 18, 1-17.  
42

43 (31) Frutos, S., Hernandez, J. L., Otero, A., Calvis, C., Adan, J., Mitjans, F., and Vila-Perello, M.  
44 (2018) Site-Specific Antibody Drug Conjugates Using Streamlined Expressed Protein Ligation,  
45 *Bioconjug. Chem.* 29, 3503-3508.  
46

47  
48 (32) Muir, T. W. (2003) Semisynthesis of proteins by expressed protein ligation, *Annu. Rev.*  
49 *Biochem.* 72, 249-289.  
50

51 (33) Wang, L., Xie, J., and Schultz, P. G. (2006) Expanding the genetic code, *Annu. Rev. Biophys.*  
52 *Biomol. Struct.* 35, 225-249.  
53  
54  
55  
56  
57  
58  
59  
60

- 1  
2  
3 (34) Liu, C. C., and Schultz, P. G. (2010) Adding new chemistries to the genetic code, *Annu. Rev.*  
4 *Biochem.* 79, 413-444.  
5  
6  
7 (35) Cao, Y., Axup, J. Y., Ma, J. S., Wang, R. E., Choi, S., Tardif, V., Lim, R. K., Pugh, H. M.,  
8 Lawson, B. R., Welzel, G., Kazane, S. A., Sun, Y., Tian, F., Srinagesh, S., Javahishvili, T., Schultz,  
9 P. G., and Kim, C. H. (2015) Multiformat T-cell-engaging bispecific antibodies targeting human  
10 breast cancers, *Angew. Chem. Int. Ed. Engl.* 54, 7022-7027.  
11  
12 (36) Lyu, Z., Kang, L., Buuh, Z. Y., Jiang, D., McGuth, J. C., Du, J., Wissler, H. L., Cai, W., and  
13 Wang, R. E. (2018) A Switchable Site-Specific Antibody Conjugate, *ACS Chem. Biol.* 13, 958-  
14 964.  
15  
16  
17 (37) Jackson, D., Atkinson, J., Guevara, C. I., Zhang, C., Kery, V., Moon, S. J., Virata, C., Yang,  
18 P., Lowe, C., Pinkstaff, J., Cho, H., Knudsen, N., Manibusan, A., Tian, F., Sun, Y., Lu, Y., Sellers,  
19 A., Jia, X. C., Joseph, I., Anand, B., Morrison, K., Pereira, D. S., and Stover, D. (2014) In vitro  
20 and in vivo evaluation of cysteine and site specific conjugated herceptin antibody-drug conjugates,  
21 *PLoS One* 9, e83865.  
22  
23  
24 (38) Tian, F., Lu, Y., Manibusan, A., Sellers, A., Tran, H., Sun, Y., Phuong, T., Barnett, R., Hehli,  
25 B., Song, F., DeGuzman, M. J., Ensari, S., Pinkstaff, J. K., Sullivan, L. M., Biroc, S. L., Cho, H.,  
26 Schultz, P. G., DiJoseph, J., Dougher, M., Ma, D., Dushin, R., Leal, M., Tchistiakova, L., Feyfant,  
27 E., Gerber, H. P., and Sapra, P. (2014) A general approach to site-specific antibody drug  
28 conjugates, *Proc. Natl. Acad. Sci. U S A* 111, 1766-1771.  
29  
30  
31 (39) Wu, Y., Zhu, H., Zhang, B., Liu, F., Chen, J., Wang, Y., Wang, Y., Zhang, Z., Wu, L., Si, L.,  
32 Xu, H., Yao, T., Xiao, S., Xia, Q., Zhang, L., Yang, Z., and Zhou, D. (2016) Synthesis of Site-  
33 Specific Radiolabeled Antibodies for Radioimmunotherapy via Genetic Code Expansion,  
34 *Bioconjug. Chem.* 27, 2460-2468.  
35  
36  
37 (40) Wu, N., Kang, C. S., Sin, I., Ren, S., Liu, D., Ruthengael, V. C., Lewis, M. R., and Chong,  
38 H. S. (2016) Promising bifunctional chelators for copper 64-PET imaging: practical (64)Cu  
39 radiolabeling and high in vitro and in vivo complex stability, *J. Biol. Inorg. Chem.* 21, 177-184.  
40  
41  
42 (41) Shokeen, M., and Anderson, C. J. (2009) Molecular imaging of cancer with copper-64  
43 radiopharmaceuticals and positron emission tomography (PET), *Acc. Chem. Res.* 42, 832-841.  
44  
45  
46 (42) Nayak, T. K., and Brechbiel, M. W. (2009) Radioimmunoimaging with longer-lived positron-  
47 emitting radionuclides: potentials and challenges, *Bioconjug. Chem.* 20, 825-841.  
48  
49  
50 (43) Cutler, C. S., Hennkens, H. M., Sisay, N., Huclier-Markai, S., and Jurisson, S. S. (2013)  
51 Radiometals for combined imaging and therapy, *Chem. Rev.* 113, 858-883.  
52  
53  
54 (44) de Sa, A., Bonnet, C. S., Geraldes, C. F., Toth, E., Ferreira, P. M., and Andre, J. P. (2013)  
55 Thermodynamic stability and relaxation studies of small, triaza-macrocyclic Mn(II) chelates,  
56 *Dalton Trans.* 42, 4522-4532.  
57  
58  
59  
60

1  
2  
3 (45) Mate, G., Simecek, J., Pniok, M., Kertesz, I., Notni, J., Wester, H. J., Galuska, L., and  
4 Hermann, P. (2015) The influence of the combination of carboxylate and phosphinate pendant  
5 arms in 1,4,7-triazacyclononane-based chelators on their  $^{68}\text{Ga}$  labelling properties, *Molecules* **20**,  
6 13112-13126.  
7

8  
9 (46) Riss, P. J., Kroll, C., Nagel, V., and Rosch, F. (2008) NODAPA-OH and NODAPA-(NCS)<sub>n</sub>:  
10 synthesis,  $^{68}\text{Ga}$ -radiolabelling and in vitro characterisation of novel versatile bifunctional  
11 chelators for molecular imaging, *Bioorg. Med. Chem. Lett.* **18**, 5364-5367.  
12

13  
14 (47) Dommerholt, J., van Rooijen, O., Borrmann, A., Guerra, C. F., Bickelhaupt, F. M., and van  
15 Delft, F. L. (2014) Highly accelerated inverse electron-demand cycloaddition of electron-deficient  
16 azides with aliphatic cyclooctynes, *Nat. Commun.* **5**, 5378.  
17

18 (48) Stasiuk, G. J., Tamang, S., Imbert, D., Poillot, C., Giardiello, M., Tisseyre, C., Barbier, E. L.,  
19 Fries, P. H., de Waard, M., Reiss, P., and Mazzanti, M. (2011) Cell-permeable Ln(III) chelate-  
20 functionalized InP quantum dots as multimodal imaging agents, *ACS Nano* **5**, 8193-8201.  
21

22  
23 (49) Badescu, G., Bryant, P., Bird, M., Henseleit, K., Swierkosz, J., Parekh, V., Tommasi, R.,  
24 Pawlisz, E., Jurlewicz, K., Farys, M., Camper, N., Sheng, X., Fisher, M., Grygorash, R., Kyle, A.,  
25 Abhilash, A., Frigerio, M., Edwards, J., and Godwin, A. (2014) Bridging disulfides for stable and  
26 defined antibody drug conjugates, *Bioconjug. Chem.* **25**, 1124-1136.  
27

28  
29 (50) Qi, J., Ye, X., Ren, G., Kan, F., Zhang, Y., Guo, M., Zhang, Z., and Li, D. (2014)  
30 Pharmacological efficacy of anti-IL-1 $\beta$  scFv, Fab and full-length antibodies in treatment of  
31 rheumatoid arthritis, *Mol. Immunol.* **57**, 59-65.  
32

33 (51) Boyerinas, B., Jochems, C., Fantini, M., Heery, C. R., Gulley, J. L., Tsang, K. Y., and Schlom,  
34 J. (2015) Antibody-Dependent Cellular Cytotoxicity Activity of a Novel Anti-PD-L1 Antibody  
35 Avelumab (MSB0010718C) on Human Tumor Cells, *Cancer Immunol. Res.* **3**, 1148-1157.  
36

37  
38 (52) Kim, C. H., Axup, J. Y., Lawson, B. R., Yun, H., Tardif, V., Choi, S. H., Zhou, Q., Dubrovskaya,  
39 A., Biroc, S. L., Marsden, R., Pinstaff, J., Smider, V. V., and Schultz, P. G. (2013) Bispecific small  
40 molecule-antibody conjugate targeting prostate cancer, *Proc. Natl. Acad. Sci. U S A* **110**, 17796-  
41 17801.  
42

43 (53) Axup, J. Y., Bajjuri, K. M., Ritland, M., Hutchins, B. M., Kim, C. H., Kazane, S. A., Halder,  
44 R., Forsyth, J. S., Santidrian, A. F., Stafin, K., Lu, Y., Tran, H., Seller, A. J., Biroc, S. L., Szydlak,  
45 A., Pinkstaff, J. K., Tian, F., Sinha, S. C., Felding-Habermann, B., Smider, V. V., and Schultz, P.  
46 G. (2012) Synthesis of site-specific antibody-drug conjugates using unnatural amino acids, *Proc.*  
47 *Natl. Acad. Sci. U S A* **109**, 16101-16106.  
48  
49

50 (54) Kern, J. C., Cancilla, M., Dooney, D., Kwasnjuk, K., Zhang, R., Beaumont, M., Figueroa, I.,  
51 Hsieh, S., Liang, L., Tomazela, D., Zhang, J., Brandish, P. E., Palmieri, A., Stivers, P., Cheng, M.,  
52 Feng, G., Geda, P., Shah, S., Beck, A., Bresson, D., Firdos, J., Gately, D., Knudsen, N., Manibusan,  
53 A., Schultz, P. G., Sun, Y., and Garbaccio, R. M. (2016) Discovery of Pyrophosphate Diesters as  
54  
55  
56  
57  
58  
59

1  
2  
3 Tunable, Soluble, and Bioorthogonal Linkers for Site-Specific Antibody-Drug Conjugates, *J. Am.*  
4 *Chem. Soc.* *138*, 1430-1445.  
5

6  
7 (55) Oller-Salvia, B. (2018) Genetic Encoding of a Non-Canonical Amino Acid for the Generation  
8 of Antibody-Drug Conjugates Through a Fast Bioorthogonal Reaction, *J. Vis. Exp.* (139).  
9

10  
11 (56) Young, D. D., Young, T. S., Jahnz, M., Ahmad, I., Spraggon, G., and Schultz, P. G. (2011)  
12 An evolved aminoacyl-tRNA synthetase with atypical polysubstrate specificity, *Biochemistry* *50*,  
13 1894-1900.  
14

15  
16 (57) Wang, R. E., Liu, T., Wang, Y., Cao, Y., Du, J., Luo, X., Deshmukh, V., Kim, C. H., Lawson,  
17 B. R., Tremblay, M. S., Young, T. S., Kazane, S. A., Wang, F., and Schultz, P. G. (2015) An  
18 immunosuppressive antibody-drug conjugate, *J. Am. Chem. Soc.* *137*, 3229-3232.  
19

20  
21 (58) Ehlerding, E. B., England, C. G., Jiang, D., Graves, S. A., Kang, L., Lacognata, S., Barnhart,  
22 T. E., and Cai, W. (2017) CD38 as a PET Imaging Target in Lung Cancer, *Mol. Pharm.* *14*, 2400-  
23 2406.  
24

25  
26 (59) Fliedner, F. P., Hansen, A. E., Jorgensen, J. T., and Kjaer, A. (2016) The use of matrigel has  
27 no influence on tumor development or PET imaging in FaDu human head and neck cancer  
28 xenografts, *BMC Med. Imaging* *16*, 5.  
29

30  
31 (60) Luo, H., England, C. G., Goel, S., Graves, S. A., Ai, F., Liu, B., Theuer, C. P., Wong, H. C.,  
32 Nickles, R. J., and Cai, W. (2017) ImmunoPET and Near-Infrared Fluorescence Imaging of  
33 Pancreatic Cancer with a Dual-Labeled Bispecific Antibody Fragment, *Mol. Pharm.* *14*, 1646-  
34 1655.  
35

36  
37 (61) Olafsen, T., and Wu, A. M. (2010) Antibody vectors for imaging, *Semin. Nucl. Med.* *40*, 167-  
38 181.  
39

40  
41 (62) DiSpirito, J. R., and Mathis, D. (2015) Immunological contributions to adipose tissue  
42 homeostasis, *Semin. Immunol.* *27*, 315-321.  
43

44  
45 (63) Nedrow, J. R., Josefsson, A., Park, S., Ranka, S., Roy, S., and Sgouros, G. (2017) Imaging of  
46 Programmed Cell Death Ligand 1: Impact of Protein Concentration on Distribution of Anti-PD-  
47 L1 SPECT Agents in an Immunocompetent Murine Model of Melanoma, *J. Nucl. Med.* *58*, 1560-  
48 1566.  
49

50  
51 (64) Tang, H., Liang, Y., Anders, R. A., Taube, J. M., Qiu, X., Mulgaonkar, A., Liu, X.,  
52 Harrington, S. M., Guo, J., Xin, Y., Xiong, Y., Nham, K., Silvers, W., Hao, G., Sun, X., Chen, M.,  
53 Hannan, R., Qiao, J., Dong, H., Peng, H., and Fu, Y. X. (2018) PD-L1 on host cells is essential for  
54 PD-L1 blockade-mediated tumor regression, *J. Clin. Invest.* *128*, 580-588.  
55  
56  
57  
58  
59  
60

**Figure Legends:**

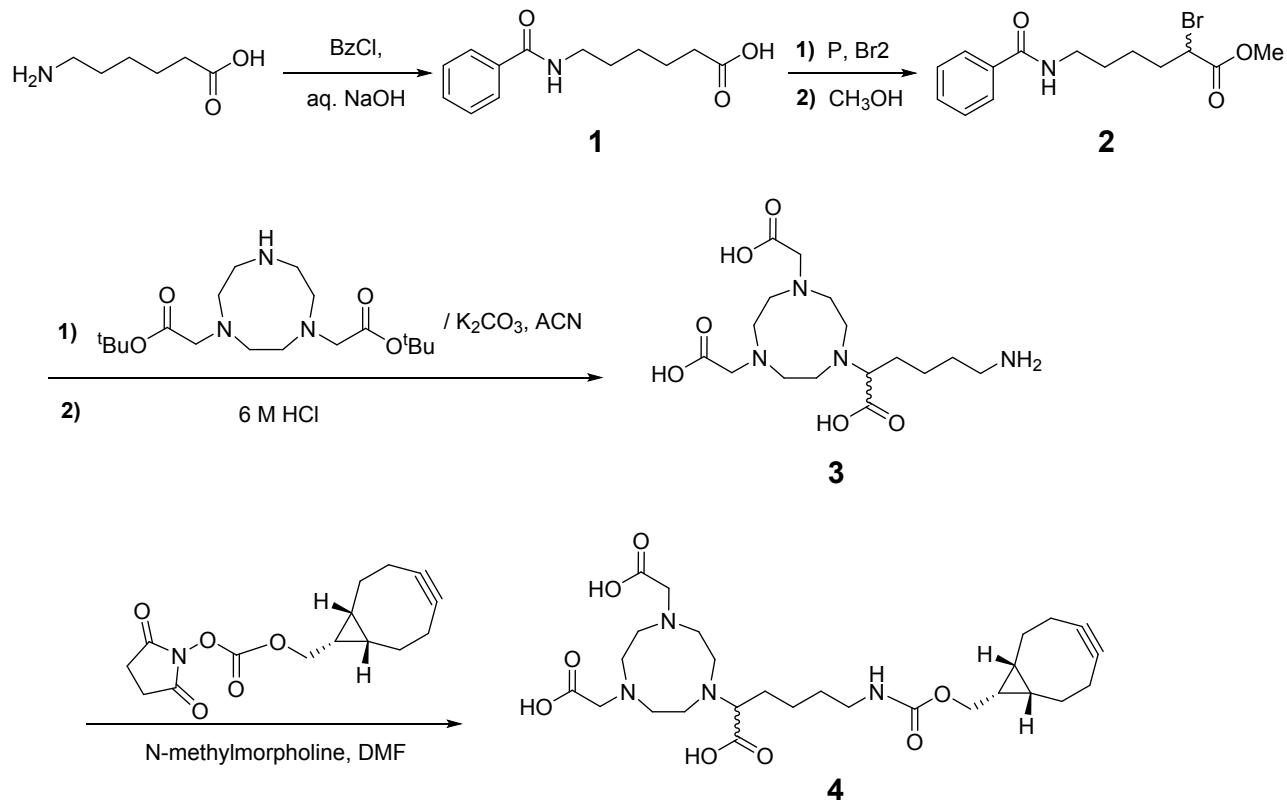
**Scheme 1.** Synthetic scheme of 1,4,7-triazacyclononane-N, N', N''-triacetic acid (NOTA) derivative with a (1R, 8S, 9S)-bicyclo[6.1.0]non-4-yn-9-ylmethylcarbamate (BCN) linker.

**Figure 1.** Synthesis and characterization of the site-specific  $^{64}\text{Cu}$ -NOTA-anti-PD-L1 Fab conjugate. (A) In silico screening with Rosetta has been performed with 23 solvent-exposed sites to determine the optimal mutation site, followed by site-directed mutagenesis to generate the anti-PD-L1 Fab (HC K129X, X = pAzF). Conjugation of this mutant with linker compound **4** will afford site-specific NOTA-anti-PD-L1 Fab conjugate **5** and its radiolabeled version, **6**. (B) ELISA analysis of the binding affinities of anti-PD-L1 Fab fragments. The  $\text{EC}_{50}$  was calculated to be  $7.8 \times 10^{-10}$  M for wild type,  $7.3 \times 10^{-10}$  M for the mutant (HC K129X, X = pAzF), and  $7.2 \times 10^{-10}$  M for conjugate **5**.

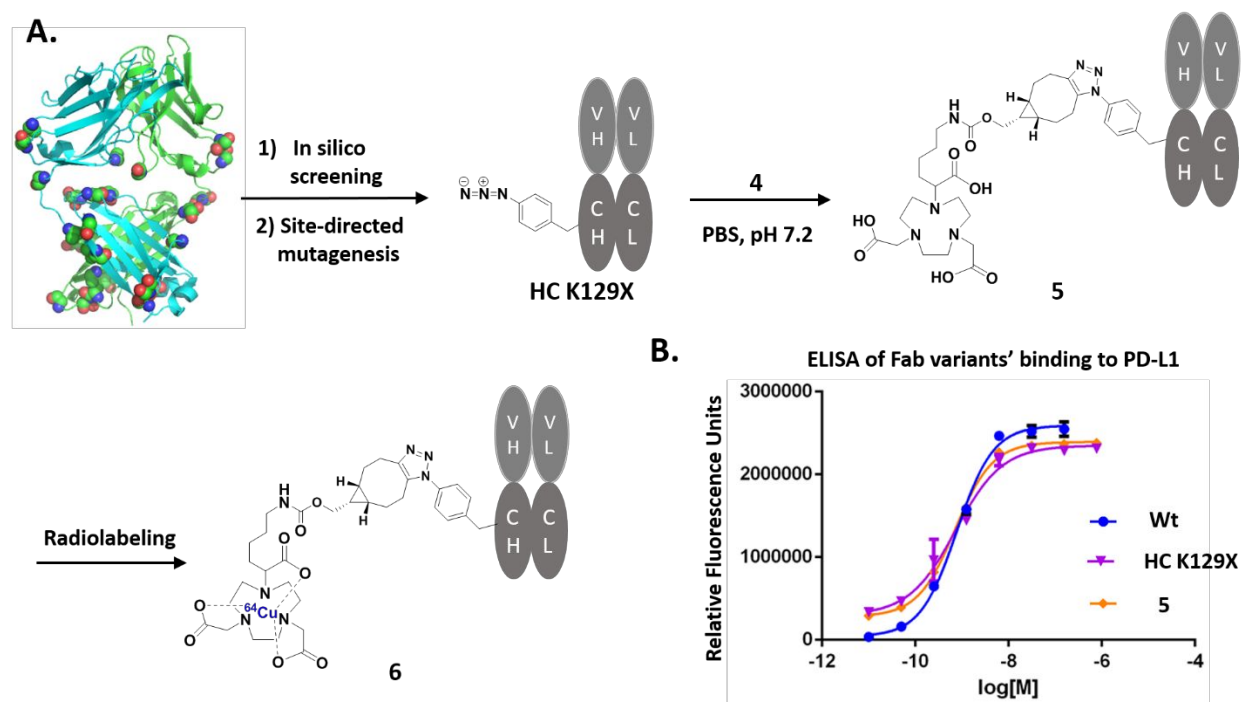
**Figure 2.** In silico screening of mutation sites on  $\alpha$ PD-L1 Fab. (A) Changes in stability  $\Delta\text{REU}$  (Rosetta energy units) for single-residue mutations to alanine (red) and phenylalanine (blue). Error bars represent standard deviations in  $\Delta\text{REU}$  across the twenty structures given by the RosettaBackrub algorithm. (B) Similar changes in stability were predicted for alanine and phenylalanine. (C) Cumulative histograms of the predicted score show that mutations at (heavy chain) H\_K129 are predicted to be the most favorable of the 23 selected residues. Predictions for the chosen negative control (light chain) L\_V202, in contrast, are not ranked as especially favorable.

**Figure 3.** *In vivo* PET imaging studies with  $^{64}\text{Cu}$ -NOTA- $\alpha$ HER2 and  $^{64}\text{Cu}$ -NOTA- $\alpha$ PD-L1 in nude mice. (A) PET scans at 15, and 45 min p.i. of  $^{64}\text{Cu}$ -NOTA- $\alpha$ HER2 (left),  $^{64}\text{Cu}$ -NOTA- $\alpha$ PD-L1 (middle), or  $^{64}\text{Cu}$ -NOTA- $\alpha$ PD-L1 with preblocking by  $\alpha$ PD-L1 w.t. (right); yellow arrowhead indicates brown fat while white arrowhead points to the spleen. (B) Tracer uptake (%ID/g) for the three imaging groups in brown fat based on quantitative region-of-interest (ROI) analysis of the PET images. (C) Tracer uptake (%ID/g) in spleen. “\*” represents  $P < 0.05$ .  $n = 3$ .

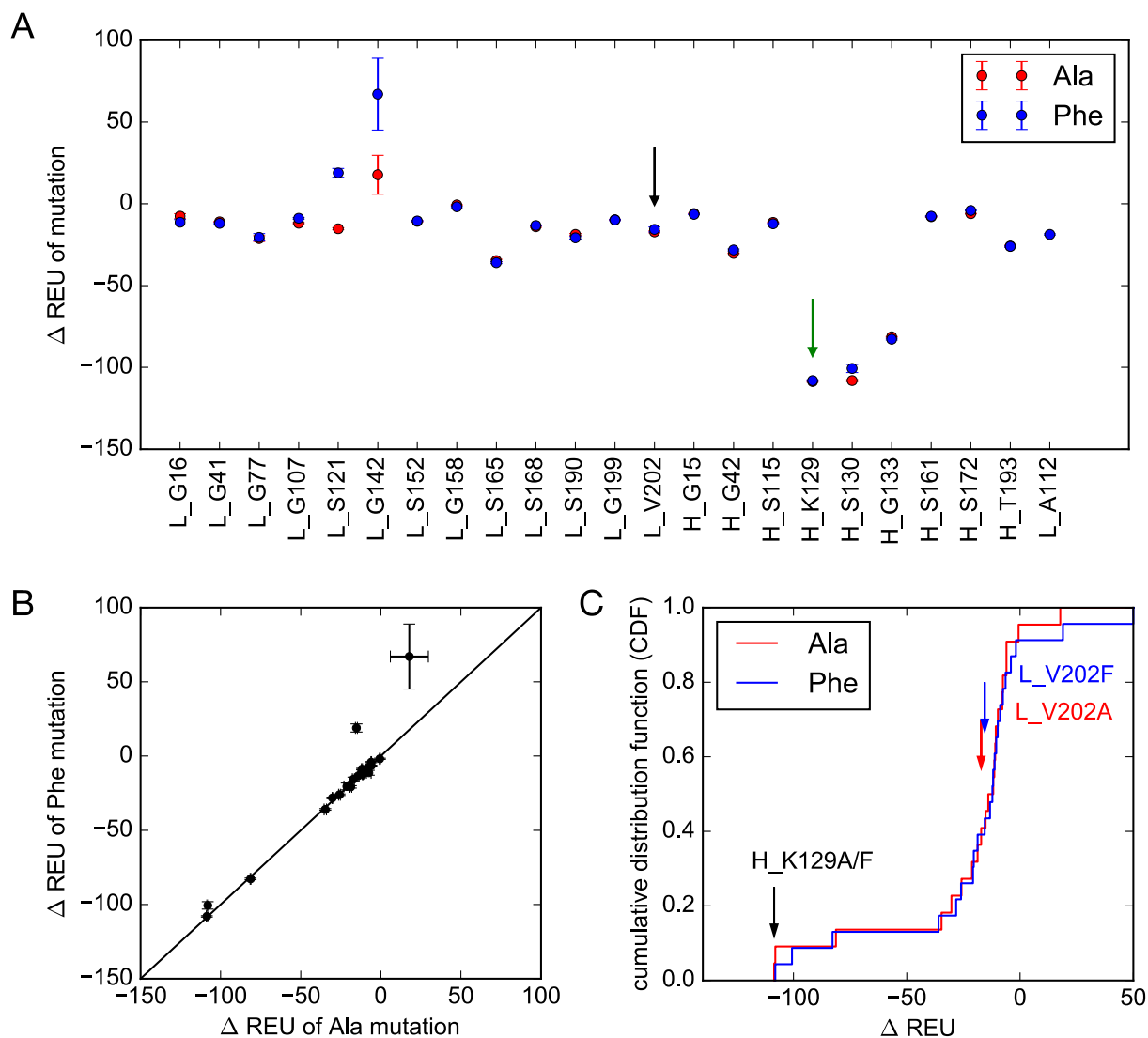
**Figure 4.** Immunofluorescent staining of brown adipose tissue for PD-L1 expression (red), and spleen tissue for PD-L1 (cyan) and CD45 (green) expressions. Nuclei (blue) were stained as controls.



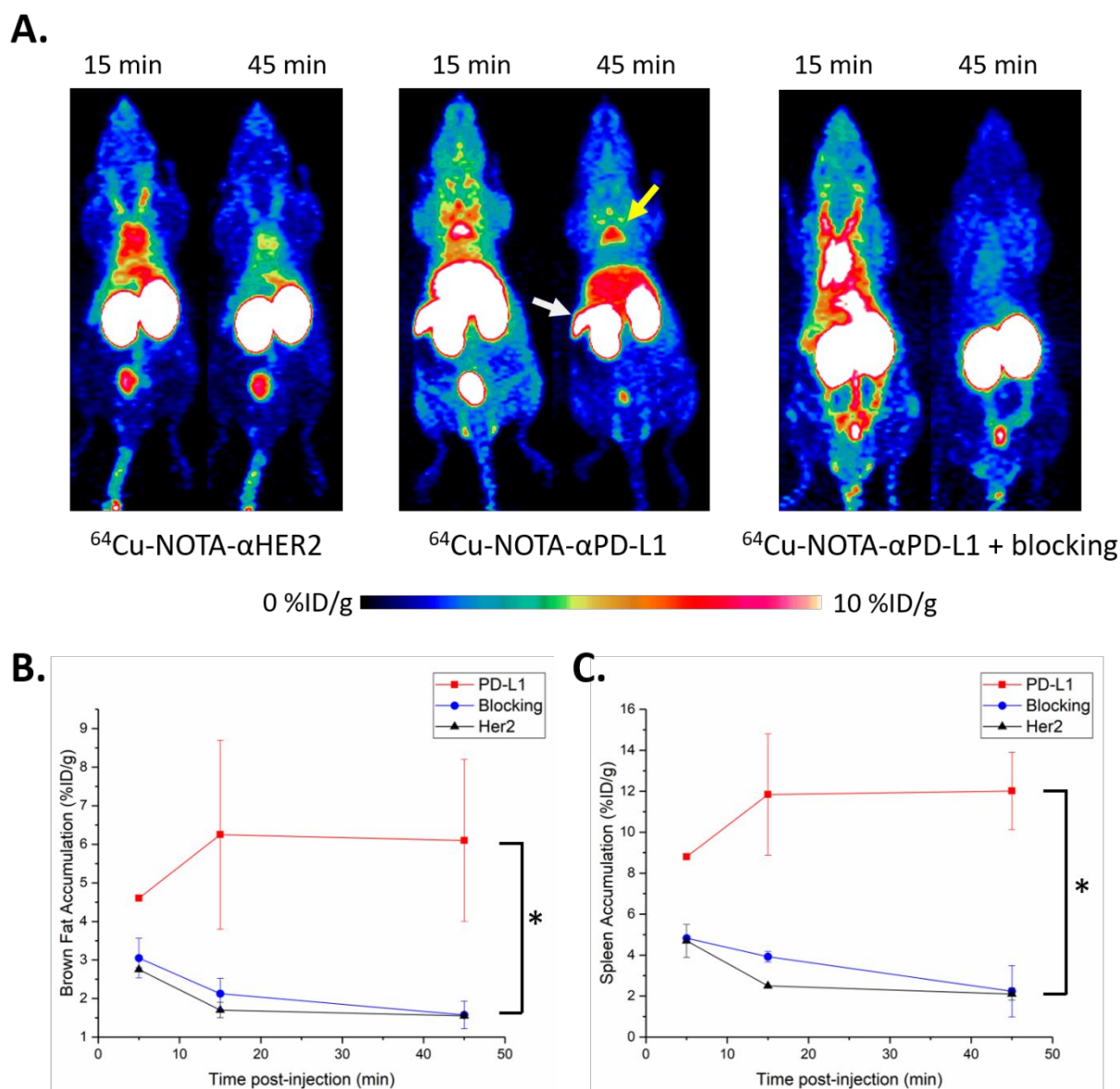
**Scheme 1** – Synthetic scheme of 1,4,7-triazacyclononane-N, N', N''-triacetic acid (NOTA) derivative with a (1R, 8S, 9S)-bicyclo[6.1.0]non-4-yn-9-ylmethylcarbamate (BCN) linker.



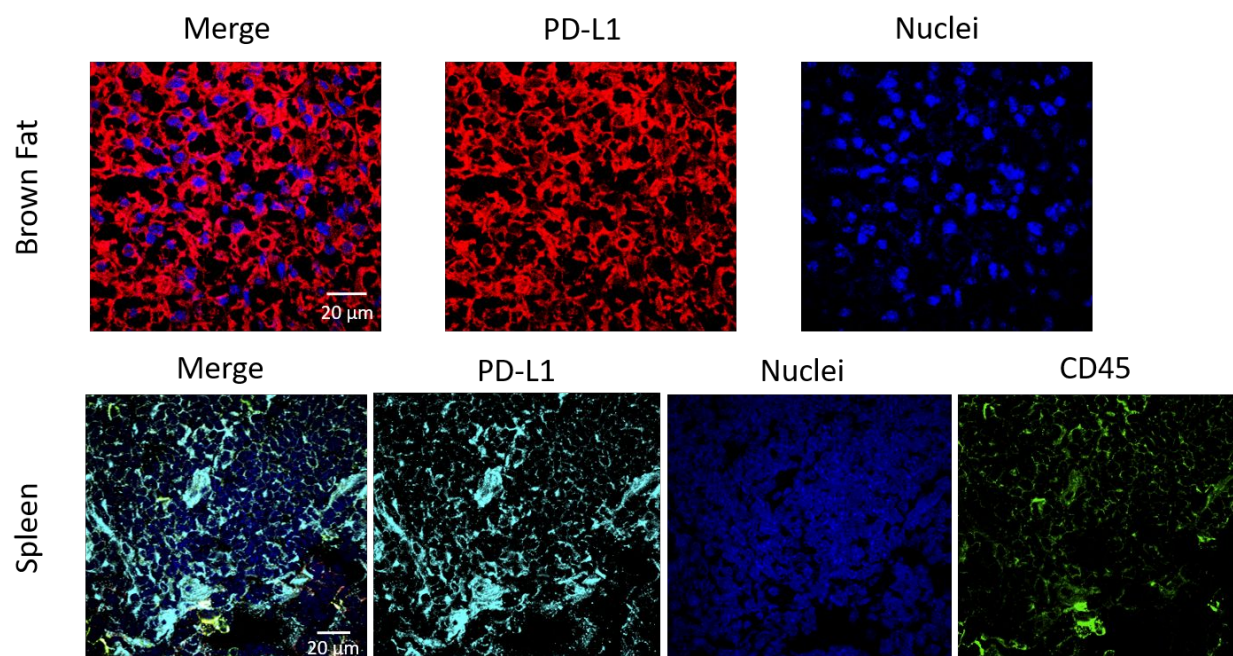
**Figure 1.** Synthesis and characterization of the site-specific <sup>64</sup>Cu-NOTA-anti-PD-L1 Fab conjugate. (A) In silico screening with Rosetta has been performed with 23 solvent-exposed sites to determine the optimal mutation site, followed by site-directed mutagenesis to generate the anti-PD-L1 Fab (HC K129X, X = pAzF). Conjugation of this mutant with linker compound **4** will afford site-specific NOTA-anti-PD-L1 Fab conjugate **5** and its radiolabeled version, **6**. (B) ELISA analysis of the binding affinities of anti-PD-L1 Fab fragments. The EC<sub>50</sub> was calculated to be 7.8 × 10<sup>-10</sup> M for wild type, 7.3 × 10<sup>-10</sup> M for the mutant (HC K129X, X = pAzF), and 7.2 × 10<sup>-10</sup> M for conjugate **5**.



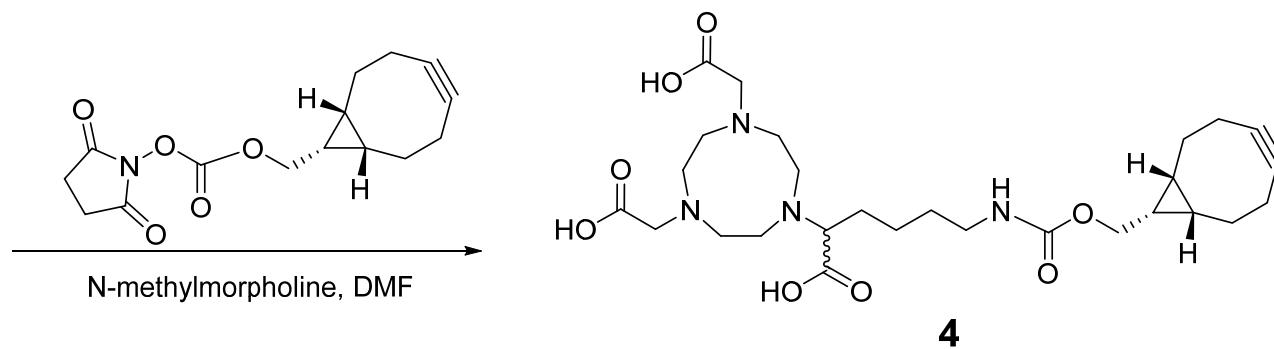
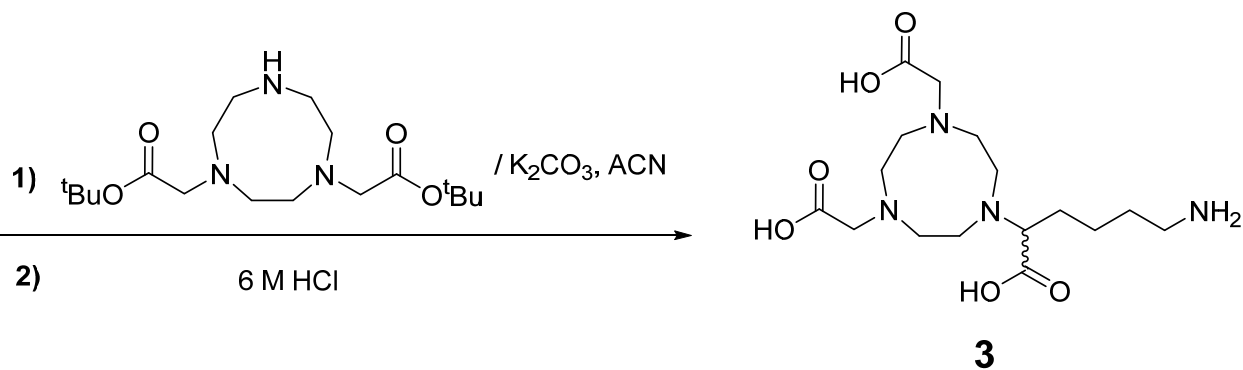
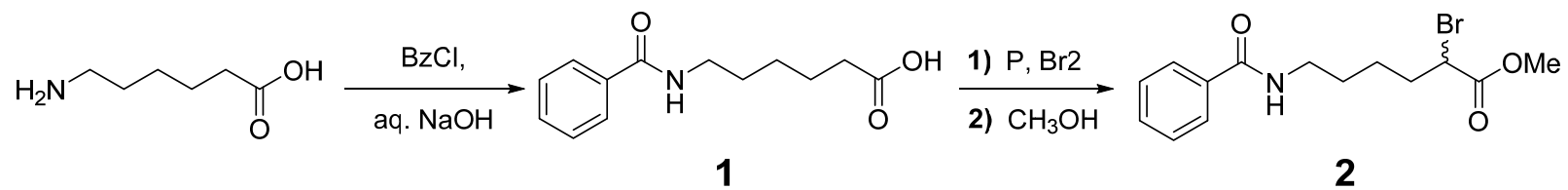
**Figure 2.** In silico screening of mutation sites on  $\alpha$ PD-L1 Fab. (A) Changes in stability  $\Delta$ REU (Rosetta energy units) for single-residue mutations to alanine (red) and phenylalanine (blue). Error bars represent standard deviations in  $\Delta$ REU across the twenty structures given by the RosettaBackrub algorithm. (B) Similar changes in stability were predicted for alanine and phenylalanine. (C) Cumulative histograms of the predicted score show that mutations at (heavy chain) H\_K129 are predicted to be the most favorable of the 23 selected residues. Predictions for the chosen negative control (light chain) L\_V202, in contrast, are not ranked as especially favorable.



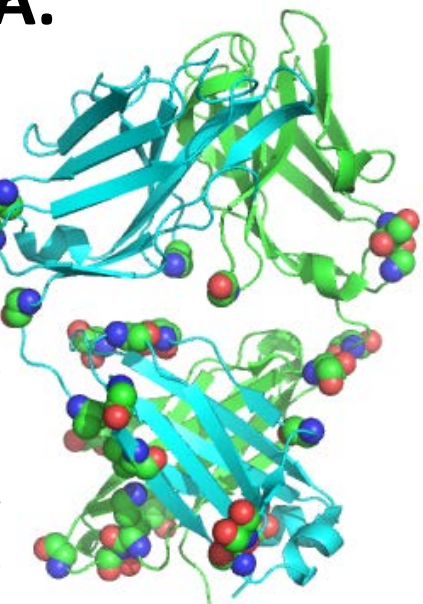
**Figure 3.** *In vivo* PET imaging studies with  $^{64}\text{Cu-NOTA-}\alpha\text{HER2}$  and  $^{64}\text{Cu-NOTA-}\alpha\text{PD-L1}$  in nude mice. (A) PET scans at 15, and 45 min p.i. of  $^{64}\text{Cu-NOTA-}\alpha\text{HER2}$  (left),  $^{64}\text{Cu-NOTA-}\alpha\text{PD-L1}$  (middle), or  $^{64}\text{Cu-NOTA-}\alpha\text{PD-L1}$  with preblocking by  $\alpha\text{PD-L1}$  w.t. (right); yellow arrowhead indicates brown fat while white arrowhead points to the spleen. (B) Tracer uptake (%ID/g) for the three imaging groups in brown fat based on quantitative region-of-interest (ROI) analysis of the PET images. (C) Tracer uptake (%ID/g) in spleen. “\*” represents  $P < 0.05$ .  $n = 3$ .



**Figure 4.** Immunofluorescent staining of brown adipose tissue for PD-L1 expression (red), and spleen tissue for PD-L1 (cyan) and CD45 (green) expressions. Nuclei (blue) were stained as controls.

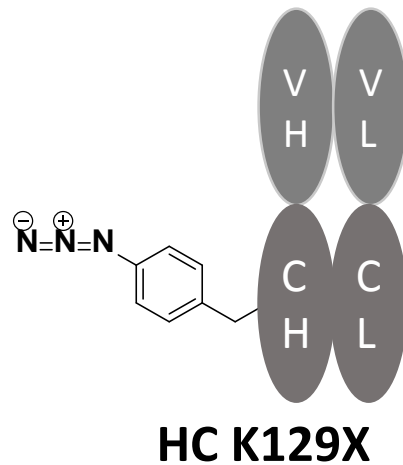


A.

1  
2  
3  
4  
5  
6  
7  
8  
9  
10  
11  
12  
13  
14  
15  
16  
17  
18  
19  
20  
21  
22  
23  
24  
25  
26  
27  
28  
29  
30  
31  
32  
33  
34  
35  
36  
37  
38  
39  
40  
41

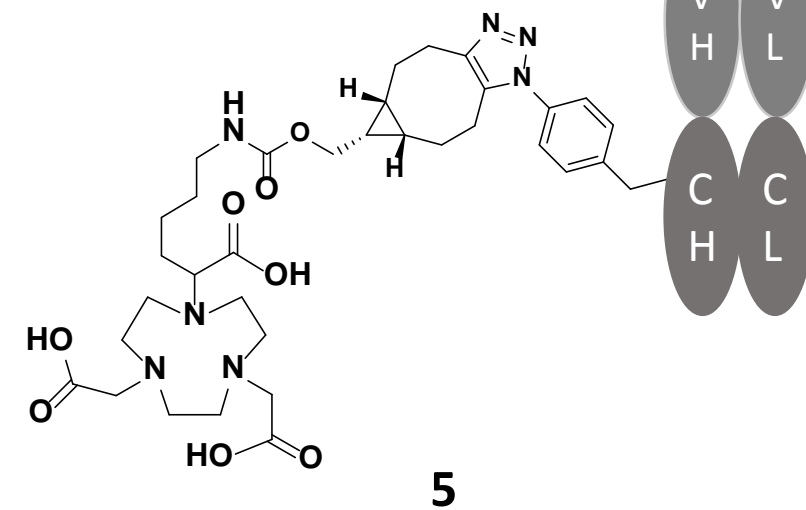
1) In silico  
screening

2) Site-directed  
mutagenesis

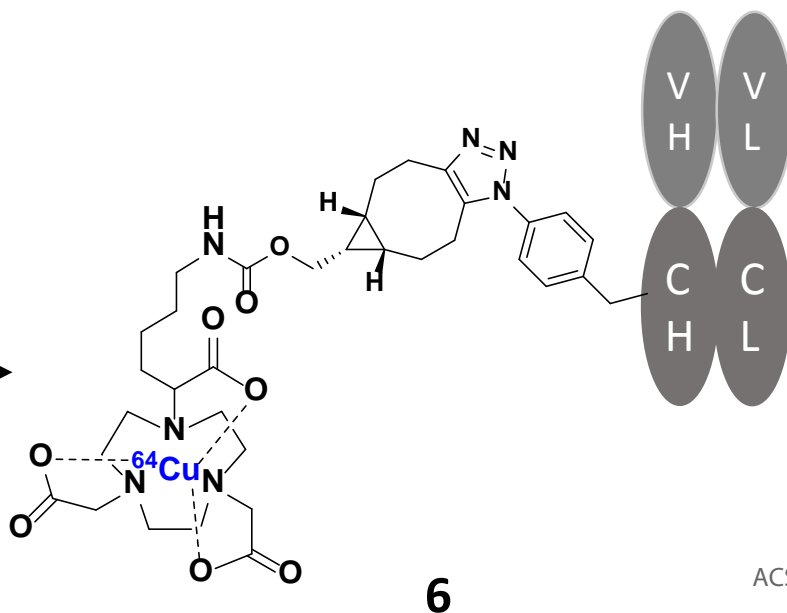


4

PBS, pH 7.2



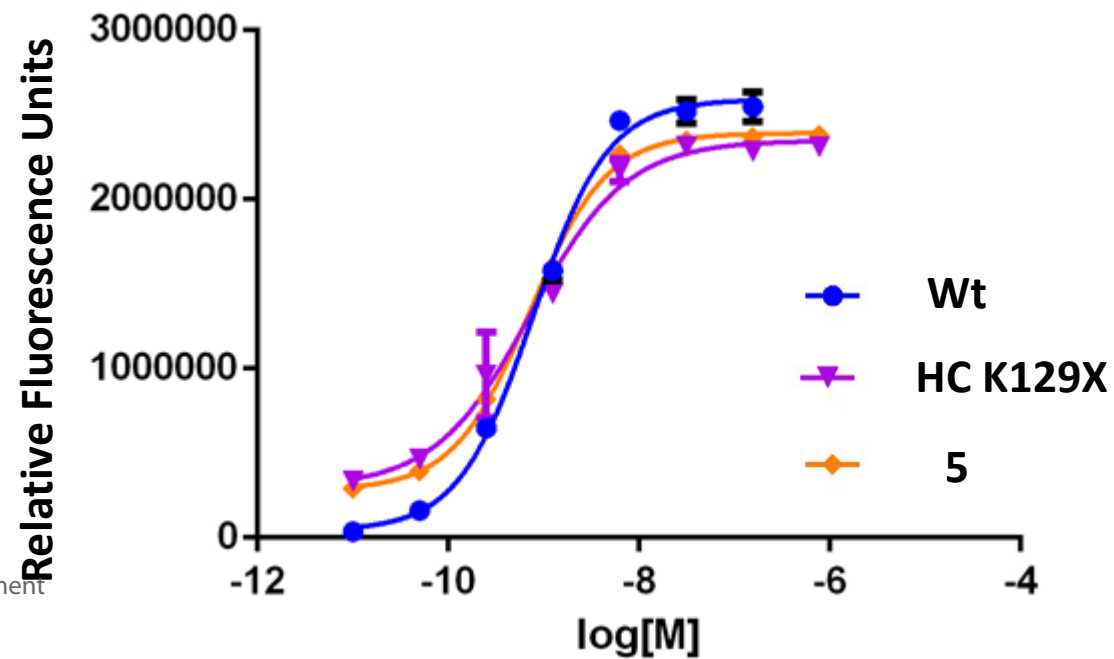
Radiolabeling

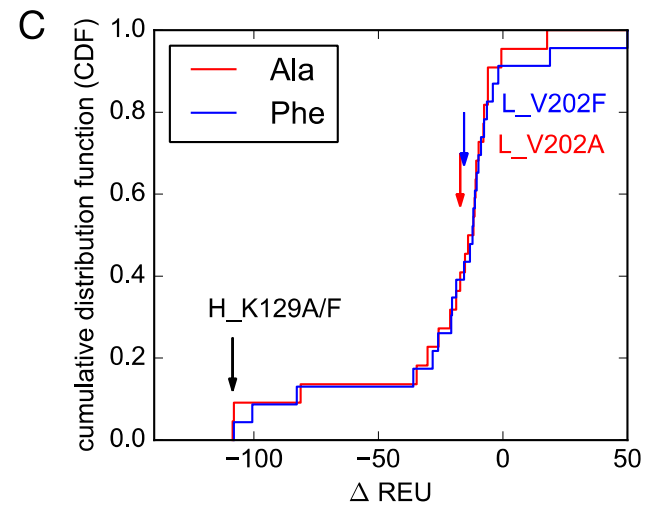
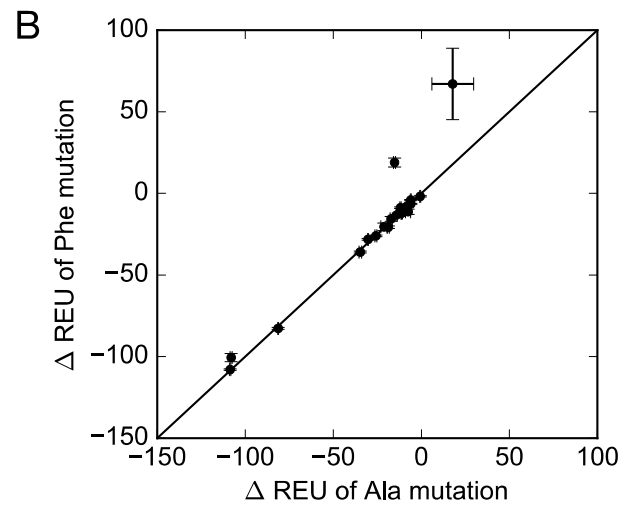
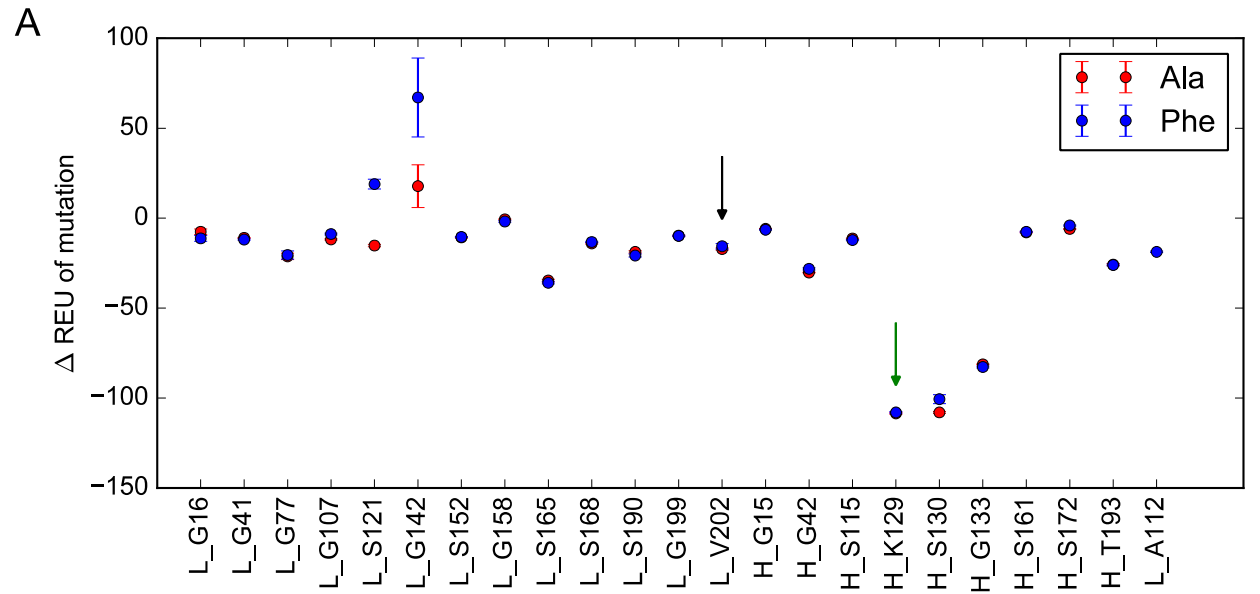


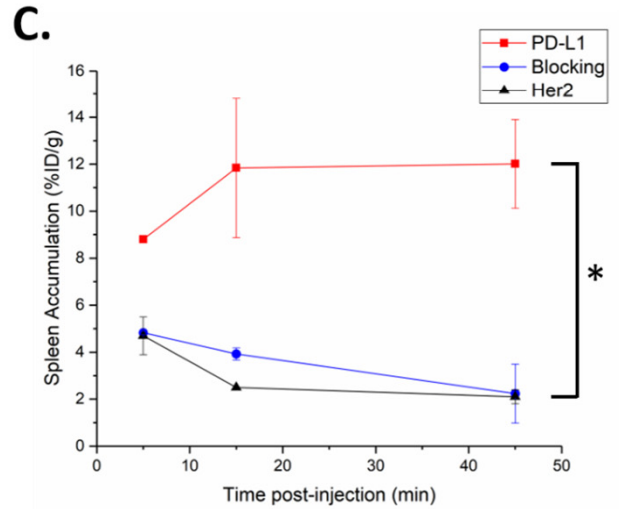
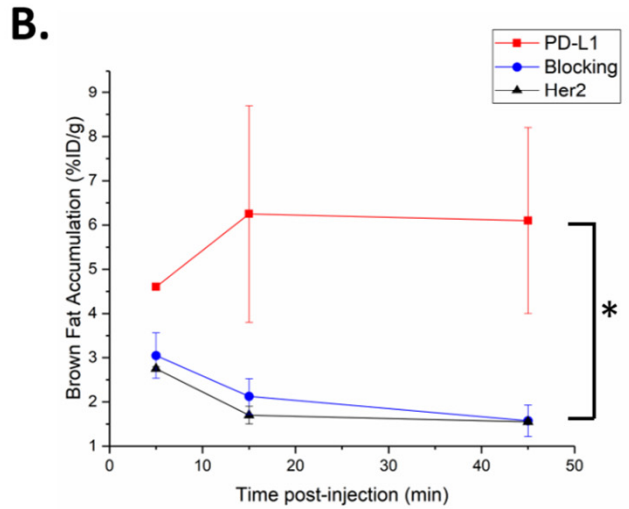
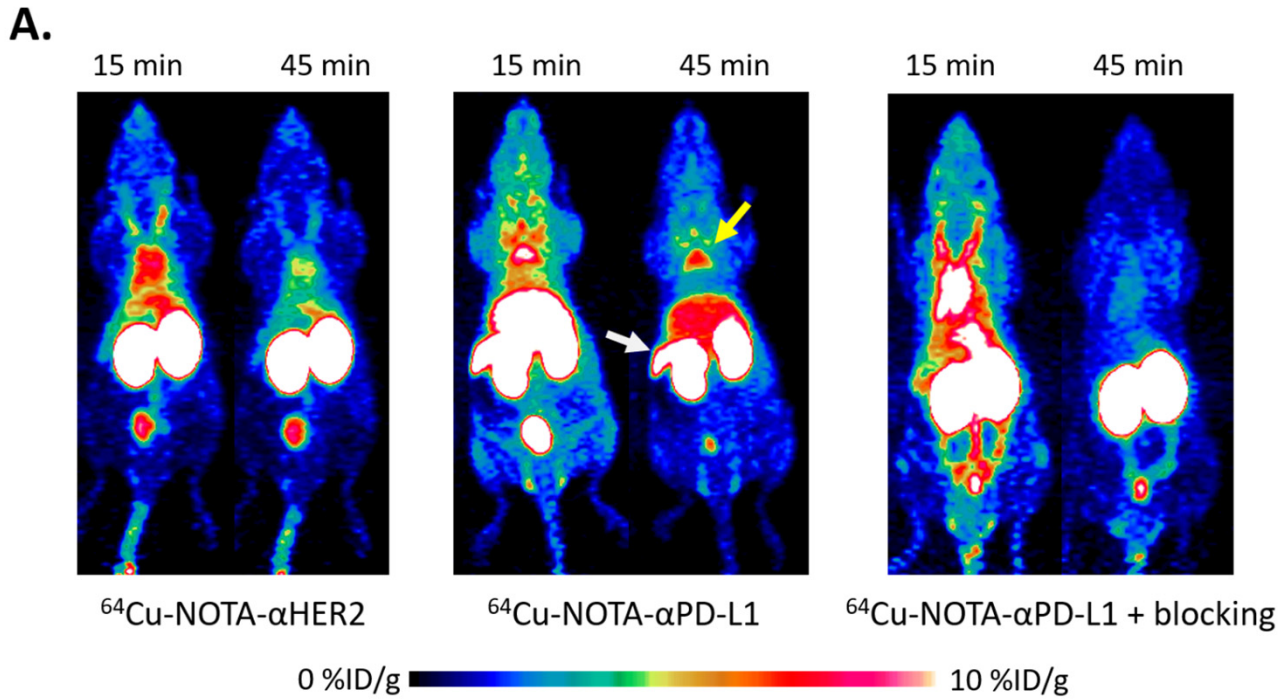
ACS Paragon Plus Environment

B.

ELISA of Fab variants' binding to PD-L1



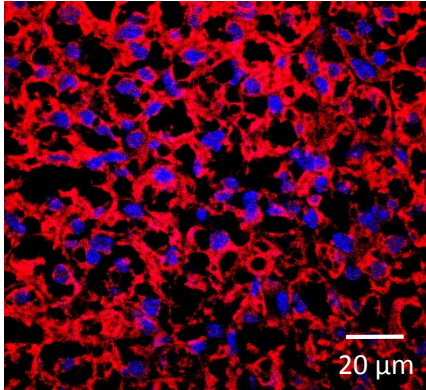




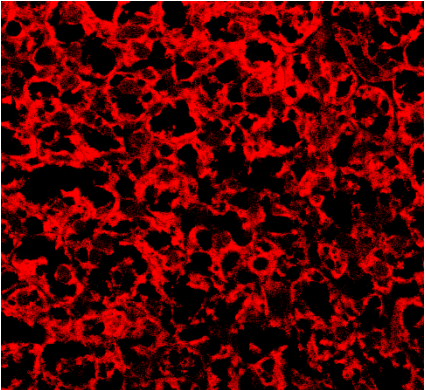
1  
2  
3  
4  
5  
6  
7  
8  
9  
10  
11  
12  
13  
14  
15  
16  
17  
18  
19  
20  
21  
22  
23  
24  
25  
26  
27  
28  
29  
30  
31  
32  
33  
34  
35  
36  
37  
38  
39  
40  
41

Brown Fat

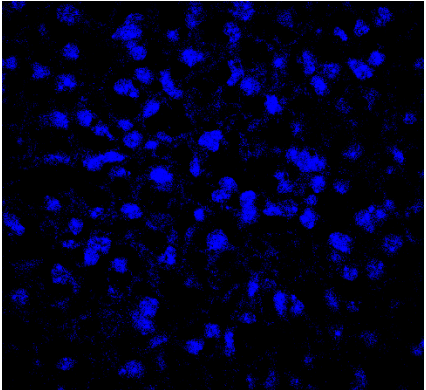
Merge



PD-L1

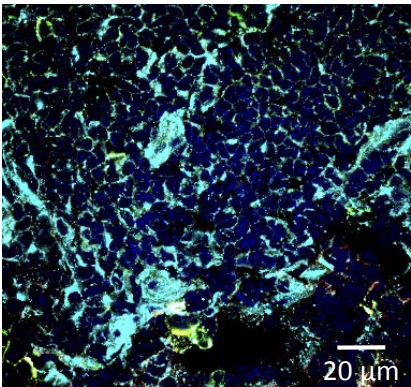


Nuclei

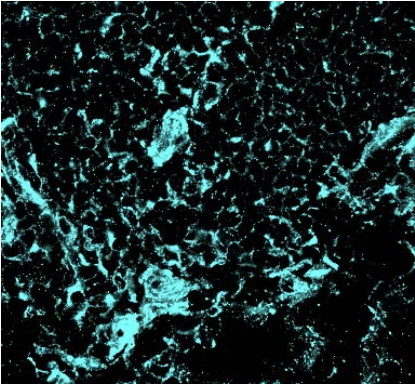


Spleen

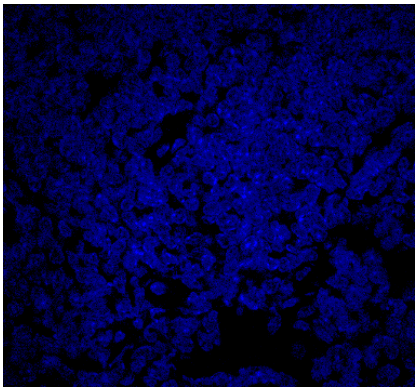
Merge



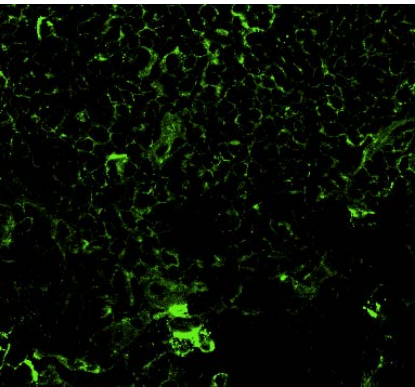
PD-L1

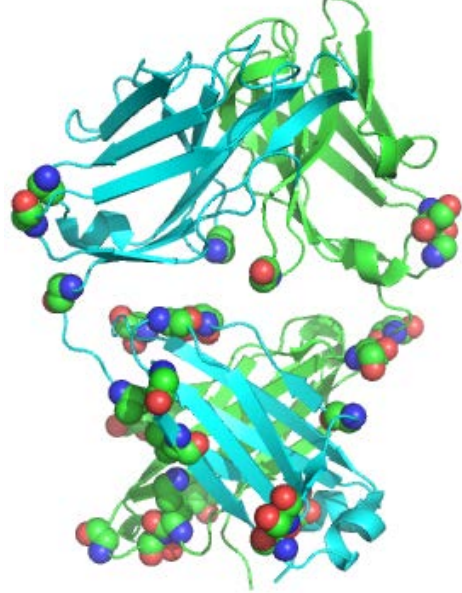


Nuclei



CD45

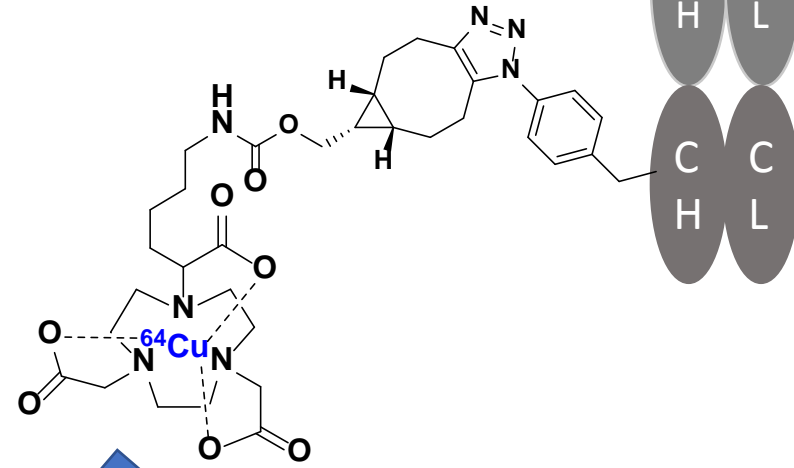




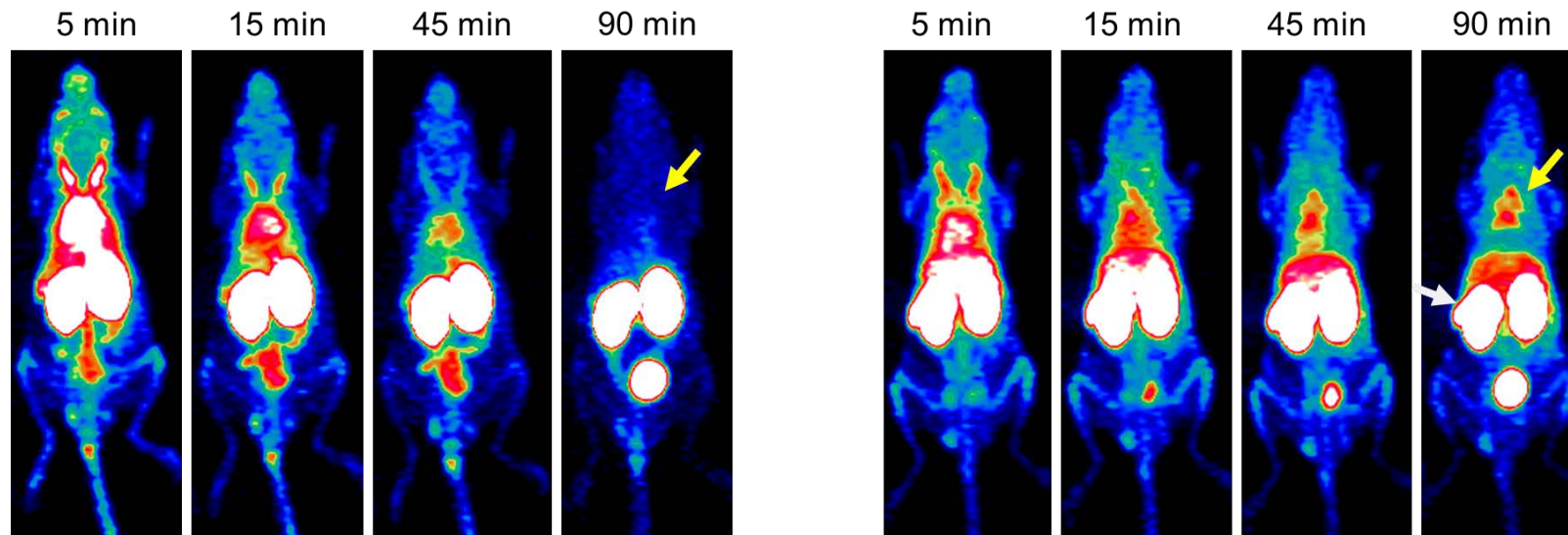
1) In silico screening



2) Site-specific mutagenesis, conjugation & radiolabeling



In vivo PET imaging



<sup>64</sup>Cu-NOTA-αHer2

ACS Paragon Plus Environment

<sup>64</sup>Cu-NOTA-αPD-L1

0 %ID/g

15 %ID/g

1  
2  
3  
4  
5  
6  
7  
8  
9  
10  
11  
12  
13  
14  
15  
16  
17  
18  
19  
20  
21  
22  
23  
24  
25  
26  
27  
28  
29  
30  
31  
32  
33  
34  
35  
36  
37  
38  
39  
40  
41